



Dominant scales of subtidal variability in coastal hydrography of the Northern Chilean Patagonia

Diego A. Narváez^{a,b,*}, Cristian A. Vargas^{a,c}, L. Antonio Cuevas^{a,c}, Sebastián A. García-Loyola^b, Carlos Lara^{a,d}, Cristian Segura^e, Fabián J. Tapia^{b,f}, Bernardo R. Broitman^{a,g,h,1}

^a Centro para el Estudio de Forzantes Múltiples sobre Sistemas Socio-Ecológicos Marinos (MUSELS), Chile

^b Centro de Investigación Oceanográfica COPAS Sur-Austral and Departamento de Oceanografía, Facultad de Ciencias Naturales y Oceanográficas, Universidad de Concepción, Concepción, Chile

^c Laboratorio de Funcionamiento de Ecosistemas Acuáticos (LAFE), Departamento de Sistemas Acuáticos and Centro de Ciencias Ambientales - EULA, Facultad de Ciencias Ambientales, Universidad de Concepción, Concepción, Chile

^d Centro de Investigación en Recursos Naturales y Sustentabilidad (CIRENYS), Universidad Bernardo O'Higgins, Santiago, Chile

^e Instituto Tecnológico de la Mitilicultura (INTEMIT), Castro, Chile

^f Centro Interdisciplinario para la Investigación Acuícola (INCAR), Universidad de Concepción, Concepción, Chile

^g Centro de Estudios Avanzados en Zonas Áridas (CEAZA), Coquimbo, Chile

^h Departamento de Biología Marina, Facultad de Ciencias del Mar, Universidad Católica del Norte, Coquimbo, Chile

ARTICLE INFO

Keywords:

Temporal variations
Spatial variations
Coastal oceanography
Ekman transport
Chile
Patagonia
Inner Sea of Chiloé

ABSTRACT

The Chilean Patagonia, on the southeastern Pacific Ocean, is one of the largest fjord systems in the world. Its complex topography harbors an aquaculture industry that is among the top exporters of salmon and mussels worldwide. However, little is known about the scales of environmental variability of this region and how climate-related changes can alter the current conditions. This study provides a baseline understanding of the dominant scales of subtidal variability in meteorological forcing and water properties along and across the region that encompasses northern Patagonia and specifically the Inner Sea of Chiloé (ISC). We examined multiple datasets spanning multiple spatial and temporal scales. Reanalysis wind time series were combined with satellite-derived data (MODIS-Aqua) and *in situ* hydrographic records from the mussel farming industry as well as from instruments moored at various locations in the ISC. We assessed the influence of large-scale forcing on the variability of local conditions and used the assembled datasets to find modes of variability at interannual, seasonal and intraseasonal scales. The patterns of atmospheric and oceanographic variability along northern Patagonia are heterogeneous both in time and space. Long-term sea surface temperature (SST) averages revealed two areas with colder temperatures and attenuated seasonal variability that can be associated with stronger vertical mixing. These areas have been previously related to hotspots for whale sightings and might be important as bottom-up controls of Patagonian food webs. Northern Patagonia is strongly affected by large-scale processes at the South Pacific basin scale. Long-term wind data show a poleward displacement of the transition between upwelling and downwelling favorable conditions during spring-summer months for the last decade. The intraseasonal time scale was dominated by a band centered at 30 days that can be attributed to atmospheric variability driven by the Baroclinic Annular Mode (BAM), which induces the periodic mixing of the water column, but with substantial interannual variability. Variability in local conditions was found to closely track the large-scale variability, even in the small channels and bays. These findings highlight the strong connection between large-scale processes and the conditions faced by aquaculture in the ISC, and the need to consider such scales of variability - as well as climate trends - in planning and management decisions.

1. Introduction

Coastal ecosystems harbor a major fraction of the fisheries and

aquaculture activities worldwide (FAO, 2016). The Chilean Patagonia, located in the southeastern Pacific Ocean, is one of the largest fjord systems in the world, spanning ca. 1700 km from 41° S to 56° S; it has a

* Corresponding author.

E-mail address: diegonarvaez@udec.cl (D.A. Narváez).

¹ Present address: Facultad de Artes Liberales, Universidad Adolfo Ibáñez, Viña del Mar, Chile

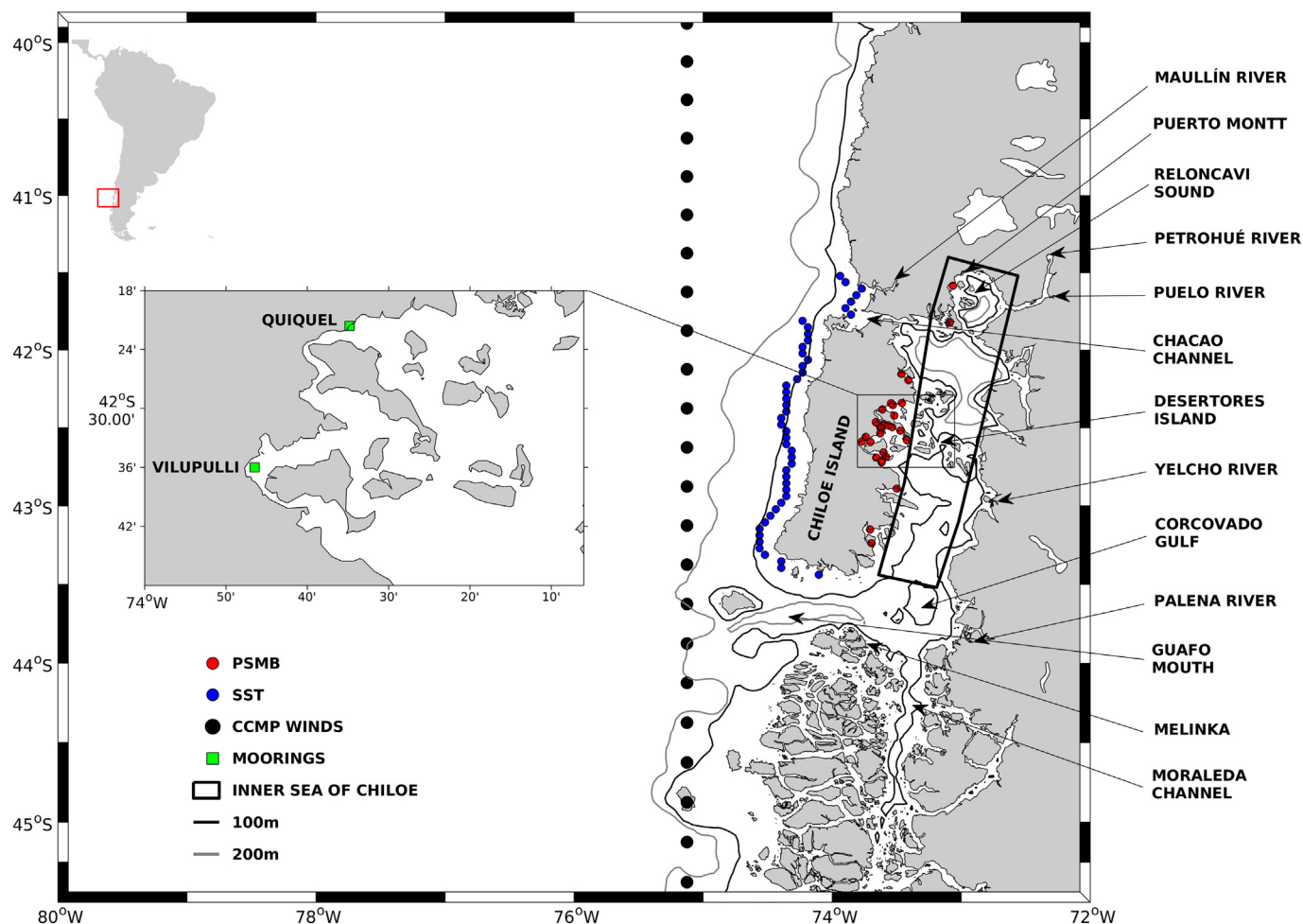


Fig. 1. Location of the study region in South America (smaller inset). The main map shows Chiloé Island, with the Chacao channel to the north and the Guafo mouth to the south. The black rectangle represents the Inner Sea of Chiloé (ISC), which is the area used to calculate the SST anomalies over eastern Chiloé. The blue dots indicate the coastal pixels used to compute SST anomalies over western Chiloé. The red dots indicate the locations where PSMB records were obtained. Black dots indicate the grid points for which wind data were obtained from CCMP Reanalysis v2 (see text for details). The 100 m and 200 m isobaths are represented by the black and gray contours, respectively. The main inset shows the central eastern coast of Chiloé with the green dots indicating the location of moored sensors. Additional data on sea surface temperature and sea level were obtained from the port of Puerto Montt. The location of rivers with the largest annual discharges of the region is also shown: Maulín ($100 \text{ m}^3/\text{s}$), Petrohué ($278 \text{ m}^3/\text{s}$), Puelo ($670 \text{ m}^3/\text{s}$), Yelcho ($360 \text{ m}^3/\text{s}$), and Palena ($130 \text{ m}^3/\text{s}$).

complex topographic and bathymetric setting including islands, bays, channels, and fjords of glacial origin (e.g., Palma and Silva, 2004; Pantoja et al., 2011; Silva and Vargas, 2014). Since the late 1980's, the region has provided ample ground for the development and geographic expansion of a large aquaculture industry, focused on salmon and mussel farming, especially in the Inner Sea of Chiloé (ISC), from $\sim 42^\circ \text{S}$ to $\sim 45^\circ \text{S}$. However, the rapid growth of aquaculture has not been matched by research aimed at providing an understanding of the main sources of environmental variability along and across the region. A key driver of the large-scale environmental variability in the region is the West Wind Drift (WWD) or South Pacific Current (SPC) (Stramma et al., 1995; Strub et al., 1998), which impinges the South American continent on northern Patagonia. Due to the WWD's influence, the region experiences a stable maritime climate, featuring a modest seasonal cycle in air temperature and abundant precipitation, with interannual variability in air temperature and precipitation responding mainly to zonal wind (Garreaud et al., 2013). Low-level westerly winds are perturbed only by the Austral Andes, and this orographic blocking enhances precipitation upstream of the catchments in the western side of the Andes Cordillera (Garreaud and Falvey, 2009; Garreaud et al., 2013). A weakening of the large-scale westerly winds over the past four decades has been consistent with an amplified seasonal cycle in local surface air temperatures around this region (Garreaud et al., 2013).

As demonstrated by the impact that a drop in the abundance of mussel larvae had on the mussel farming industry (Lara et al., 2016) and the recent occurrence of large Harmful Algal Blooms (HABs) in and around the ISC (León-Muñoz et al., 2018), environmental changes with far-reaching ecosystem impacts are not necessarily forced locally. Therefore, large to mesoscale oceanographic variability must be considered by the aquaculture industry and other human activities to reduce the impacts of extreme events for society and livelihoods. To build up the adaptive capacity of aquaculture to changing ocean conditions as well as to anthropogenic stressors around Patagonia, it is fundamental to first understand the natural variability of environmental conditions at different spatial and temporal scales. Primarily, achieving such goal involves establishing the dominant scales of spatial and temporal variability in seawater properties and patterns of water circulation within the fjords and channels of Patagonia, as well as on the adjacent continental shelf. Most of the recent research along the Patagonian fjords has focused on either broad descriptions of biological and physical properties in a regional context (e.g., Jacob et al., 2014), or local-scale process studies in specific fjord areas (e.g., Iriarte et al., 2014; Castillo et al., 2016; Pérez-Santos, 2017). Less attention has been paid to the atmospheric and oceanographic context in which Patagonian fjords and channels are embedded, and the extent to which variability in open and coastal waters – forced either locally or remotely – may

drive changes in physical-chemical conditions and productivity in economically sensitive coastal areas such as the ISC.

To provide a baseline understanding of the dominant scales of subtidal variability (> 1-day) in meteorological forcing and water properties across northern Patagonia and, more specifically, the region encompassing the ISC, we examined multiple datasets spanning multiple spatial and temporal scales. Meteorological time series from the Cross-Calibrated Multi-Platform (CCMP) reanalysis (version 2) were combined with satellite-derived data (MODIS-Aqua), time series from coastal sea level stations, and *in situ* records from the mussel farming industry as well as from instruments moored at various locations of the ISC. We assessed the connection between large-scale forcing and the variability of local conditions and identified the principal modes of variability at interannual, seasonal and intraseasonal scales in the datasets assembled for the region. A better understanding of the connection between local conditions and large-scale forcing is relevant to assess the potential effects of future climate scenarios on this highly productive and socio-economically important region.

2. Materials and methods

2.1. Study area

The study area extends from 40 to 45° S, encompassing the Inner Sea of Chilóe (ISC), which spans ca. 260 km from the Reloncaví sound to the Corcovado gulf (Fig. 1). The ISC has a steep bathymetry, with maximum depths of ~ 200 m in the main channels, and it is connected to the Pacific Ocean through the Chacao channel (41.8° S) and the Guafo mouth (43.4° S), both connections are through deep channels with no sills that could interfere with the water exchange. The Chacao channel is about 3 km wide, with maximum depths of 100 m and the Guafo mouth, 40 km wide and with maximum depth of 200 m, is the largest connection between the ISC and the Pacific Ocean. The ISC has a variable width due to the complex topography of the Chilóe Island to the west, the continental area with fjords and channels to the east, and a set of islands (Desertoires islands) bisecting the basin into a northern and a southern section (Lara et al., 2016). All of these topographic and bathymetric features modulate the effect of winds and tidal currents on the hydrodynamics of the ISC (e.g., Silva et al., 1998; Letelier et al., 2011). Seasonal variability in the wind regime has been recorded at Guafo island, just outside the Guafo mouth (see Fig. 1), with predominant southerly and southwesterly winds during the austral spring-summer and northerly and northeasterly winds during the fall-winter season (Cáceres et al., 2003). Semidiurnal tidal amplitudes increase from 1.5 m at the Guafo Mouth (Fierro et al., 2000) to about 7 m in Puerto Montt (Cáceres et al., 2003), with current velocities of up to 4 m/s in the Chacao Channel (Cáceres et al., 2003). This increase in tidal amplitude has been associated with the occurrence of tidal resonance in the ISC (Aiken, 2008; Cáceres et al., 2003).

The ISC water column is characterized by a low-salinity surface layer associated to freshwater inputs from rivers, glacial melting, and precipitation (Estuarine Water, EW) and a subsurface layer of higher salinity influenced mostly by intrusions of Sub-Antarctic Waters (SAAW) (e.g., Dávila et al., 2002; Palma and Silva, 2004) and deep intrusions of Equatorial Subsurface Waters (ESSW) (Silva and Vargas, 2014). The vertical mixing between EW and SAAW results in modified SAAW at the interface of both water masses (Sievers and Silva, 2008). The vertical salinity gradient drives an estuarine circulation with a relatively shallow halocline (Acha et al., 2004; Valle-Levinson et al., 2007; Iriarte et al., 2014), surface outflows of EW, and subsurface inflows of Sub-Antarctic Waters (SAAW) through the Guafo mouth into the ISC (Silva and Neshyba, 1979; Silva et al., 1997, 1998).

The EW are characterized by the low nitrate and phosphate concentrations contained in the oligotrophic river that drain in the basin, and the major contribution of these nutrients to the ISC is through intrusions of SAAW (Silva and Neshyba, 1979; Silva et al., 1997, 1998).

The interaction between SAAW intrusions and the EW, which is rich in dissolved silicon from rivers (Silva and Palma, 2006; Vargas et al., 2011), contributes to this highly dynamic and productive system. This region exhibits high rates of primary production, with high phytoplankton biomass (González et al., 2011; Iriarte et al., 2007), and latitudinal gradients in primary production that have been associated with changes in light attenuation and local hydrographic conditions (Jacob et al., 2014). This high productivity also explains the occurrence of large whale aggregations (mainly Blue whales, but also Sei and Humpback) in feeding grounds located near the Corcovado Gulf (Hucke-Gaete et al., 2010; Buchan and Quiñones, 2016). The extent of the effect that freshwater from the ISC may have on the biogeochemistry of the SE Pacific Ocean is mostly unknown. However, sea surface salinity data derived from satellite imagery and ARGO floats (see Saldías et al., 2018) indicate the presence of low salinity waters over a large section of the adjacent ocean throughout the year, but especially during spring-summer and fall.

2.2. Environmental data and analysis

2.2.1. Wind and climate data

We used gridded surface winds from the Cross-Calibrated Multi-Platform (CCMP). This dataset is derived from a combination of V7-RSS radiometer wind speeds, QuikSCAT, SSM/I, SSMIS, AMSR-E, TRMM, TMI, SeaWinds, WindSat and ASCAT scatterometer wind vectors, moored buoy wind data and the ERA-Interim model, using a Variational Analysis Method (VAM) to produce 6-h wind maps with 0.25° spatial resolution from 1990 to 2017 (Wentz et al., 2015). CCMP Version-2.0 vector wind analyses are produced by Remote Sensing Systems. Data are available at www.remss.com. Validations of CCMP winds against data from meteorological stations available for the study area are shown in Fig. S1 (supplementary figures). Significant correlations and matching variability suggest that CCMP wind data capture variability similar to that captured by *in situ* wind observations.

Wind stress was computed according to Kraus (1972) and Nelson (1977) for coastal CCMP grid points located immediately offshore, north, and south of the ISC (see Fig. 1) following:

$$\tau_y = \rho_a Cd (u^2 + v^2)^{1/2} v \quad (1)$$

Where ρ_a (kg/m³) is air density and Cd is a drag coefficient of 0.0013; we used this constant value of drag coefficient following Large and Pond (1981), who demonstrated that it does not generate large variations in the calculation of stresses for wind speeds below 11 m/s, and u and v are the zonal and meridional components, respectively. Wind stress along the main axis (τ_y) was then used to calculate across-shelf Ekman transport (M) at each grid point following:

$$M = \frac{\tau_y}{\rho_w f} \quad (2)$$

Where ρ_w (kg/m³) is water density and f is the Coriolis parameter (s^{-1}), and positive (negative) values of M indicate onshore (offshore) transport, i.e., downwelling (upwelling) favorable winds. The Ekman transport was estimated along the ~ 75° W meridian for a latitudinal range of 30–50° S, in order to examine alongshore and temporal changes in coastal Ekman transport during contrasting seasons, i.e., winter (May–August) and summer (December–March) months. There are no significant differences in the results choosing a meridian closer. The location (i.e., latitude) of the transition from upwelling to downwelling favorable winds during summer months was estimated for each year, and a trend analysis was performed using the least-squares method to test whether the latitude of transition had significantly changed its position over time. The trend's statistical significance was tested using the non-parametric Mann-Kendall test.

To address the effects of large-scale climate variability on regional and local-scale conditions we analyzed four climatic indices: the Pacific Decadal Oscillation (PDO), the Multivariate ENSO Index (MEI), the

Antarctic Oscillation index (AAO), also known as Southern Annular Mode (SAM), and the Madden Julian Oscillation (MJO) index. PDO data are available from the University of Washington's Joint Institute for the Study of the Atmosphere and Ocean website (research.jisao.washington.edu/pdo), MEI data, AAO and MJO indices were obtained from the NOAA's Climate Prediction Center (www.cpc.noaa.gov) and Earth System Research Laboratory, Physical Science Division (www.esrl.noaa.gov).

Cross-correlations and spectral analyses were performed following Emery and Thomson (2001). Cross-correlation analyses were used to identify associations between variables and their corresponding time lags. Spectral analysis using the Welch method and wavelets analysis following Torrence and Compo (1998) were conducted to detect the dominant frequencies of variability in the time series.

2.2.2. Satellite data

To examine the mesoscale variability of the surface ocean temperature across the ISC, we used satellite imagery produced by the MODIS-Aqua mission. Data used in our analysis corresponded to 8-day composites of Level-3 and 11 μ m SST images (4 km spatial resolution) for the period between January 2003 and August 2018. The images were monthly averaged to reduce the number of gaps due to persistent cloud coverage in this area. Anomalies of SST were estimated by subtracting climatological means computed for each month of the year. To represent the meridional pattern in SST variability along the western Chiloé, SST time series were extracted from one coastal pixel at each latitude. To avoid land influence, the fourth pixel closest to the shoreline (i.e., ~16 km offshore) was used for each latitude.

To characterize the spatial structure of SST variability across the ISC and, more specifically, the influence of seasonal fluctuations in SST, we applied harmonic analysis to monthly SST images spanning the region defined by 41–44° S and 72–76° W. From each 4 × 4 km pixel that contained good-quality data (i.e., valid data in more than 50 % of the images), we extracted the corresponding monthly time series of SST and fitted an annual harmonic signal (i.e., period of 365.25 days) using the least-squares procedure described by Emery and Thomson (2001). Amplitude of the fitted annual harmonic, as well as the residual variance (i.e., fraction of total variance in the time series that was unaccounted for by the annual harmonic) were computed for each pixel over the region and subsequently mapped. Finally, a trend analysis was performed on the residuals computed for each pixel, in order to test whether SST has significantly changed over the past 15 years. The analysis consisted of fitting a linear regression model to the residuals of each time series (i.e., pixel), which were obtained by subtracting the annual harmonic from the original monthly time series. Significance for each linear regression trend (slope) was determined using an ANOVA to test the null hypothesis that the trend is zero with an $\alpha = 0.05$.

To verify whether the patterns observed in surface temperature are influenced by fortnightly tides in the region, we compiled daily SST images collected during spring and neap tides in summer months (December through March) for the period 2003–2018. Dates corresponding to each phase of the lunar cycle were determined from the sea-level record provided by the Chilean Navy for the port of Puerto Montt. A total of ~120 images were used to estimate each spring and neap tides averages.

2.2.3. Moored instrumentation

Floating platforms were deployed at two locations on the eastern shore of Chiloé (Fig. 1): Vilupulli (southern mooring) and Quiquel (northern mooring) from August 2015 to November 2017. Both platforms were located close to mussel farms, with overall sea floor depths of 20 m and 50 m, respectively. From each platform, continuous records of temperature, salinity, chlorophyll-a fluorescence, and dissolved oxygen were obtained with a Seabird Water Quality Monitor (WQM). A Satlantic SeaFET was deployed at the same locations to measure pH; details on the calibration of pH measurements are given in Appendix A.

Both sensor arrays were deployed at 4 m below the surface, which corresponds to the mid-depth of mussel-farming vertical lines. Although both WQM and SeaFET are equipped with active and passive antifouling mechanisms, moorings were serviced (and data were downloaded) on a monthly basis. We complemented these fixed-depth continuous records with CTD profiles obtained at each location prior to servicing the sensors, in order to compare the conditions at 4 m depth with the entire water column, and to assess potential inconsistencies or drift in the continuous measurements.

As for data processing, daily averages were calculated after removing outliers and parts of the records corresponding to servicing times. When servicing times lasted less than 1–2 days, data gaps in the daily time series were filled by simple linear interpolation. Larger data gaps were due to technical problems with the equipment. All of the figures and analyses were performed on the daily averages, with the exception of the pH calibration (see supplementary figures).

2.2.4. Environmental monitoring programs for aquaculture

Following requirements from foreign markets, the Chilean health authority requires that shellfish aquaculture producers conduct periodic (i.e., monthly or bi-monthly) point surveys of physical-biological and sanitary parameters in a program called “Programa de Sanidad de Moluscos Bivalvos” (hereafter PSMB). PSMB data available for the ISC region were compiled by the Instituto Tecnológico de la Mitilicultura (www.intemit.cl), totaling 51 monitoring stations that were sampled regularly from 2008 to mid-2015. Data were obtained from the collaborative monitoring program led by the mussel aquaculture industry association (AMI-Chile) from which we selected information on temperature, salinity, dissolved oxygen, and pH. Since the temporal and spatial coverage of PSMB information is extremely uneven, a thorough process of quality control was conducted for every location to remove outliers and ensure data consistency and quality. From the 51 locations available initially, 23 locations with longer and better-quality records were selected to represent local variability across the ISC. Monthly averages were calculated when more than 2 PSMB measurements were conducted within a month at a given site. The precision for the different parameters reported is variable, as it involves a number of different people with different sensors operating across an extensive region (see Fig. 1), with sampling protocols that were not documented. Despite all of these shortcomings, PSMB water temperature data were regarded as reliable, given the robustness of temperature measurements, to be included in our analyses as a way to connect satellite information with local conditions amid the complex geographic setting of the ISC.

2.2.5. Additional data

Time series of sea level height and water temperature collected at the port of Puerto Montt from January 2000 to December 2016 were obtained from the Chilean Navy's Centro Nacional de Datos Hidrográficos y Oceanográficos (CENDHOC).

3. Results

3.1. Climatological variability

The 15-year average SST field from MODIS-Aqua revealed a heterogeneous spatial structure in the region, with warmer oceanic waters in the northwestern section and cooler waters in coastal areas as well as in the southern section of the ISC. A strong thermal gradient ((2–3° C) between the southern and northern sections of the ISC (i.e., from Corcovado Gulf to Reloncaví Sound, Fig. 2A) was apparent. Temporal variability in SST - as shown by the field of SST standard deviations (STD) - was greater in the warmer regions, especially at semi-closed areas such as fjords and bays as well as in offshore waters (Fig. 2B). To some extent, the spatial pattern observed in the amplitude of the annual cycle was consistent with that shown by the climatological mean and STD (Fig. 2C), suggesting that a large fraction of SST variability in the

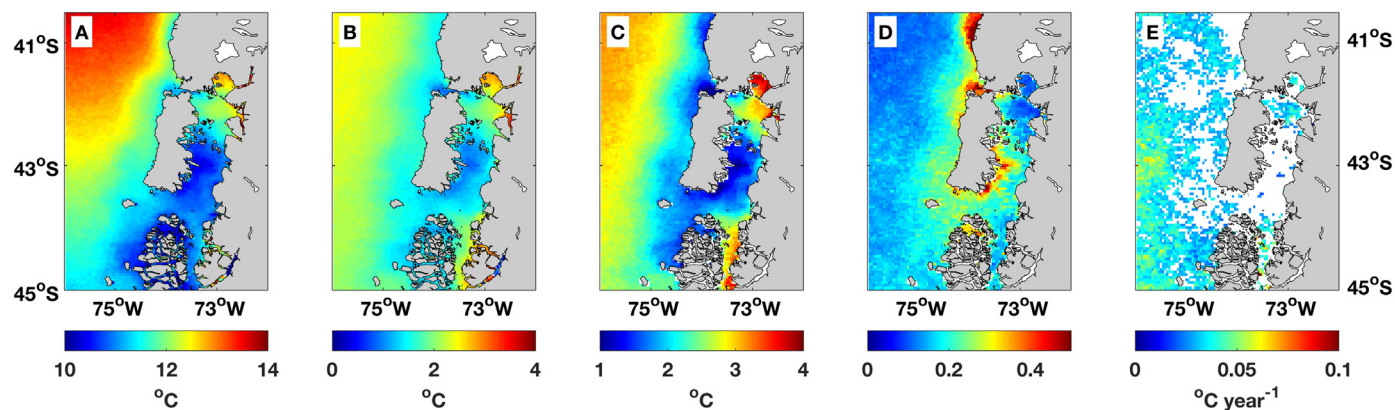


Fig. 2. Long-term (2003–2018) mean (A) and standard deviation (B) of sea surface temperature (SST) across the Chiloé region. The spatial structure of the amplitude of the annual cycle of SST (C) and the fraction of the total variance unaccounted for by the annual cycle (D) were estimated from harmonic analysis. Locations (pixels) where the linear trend in the residual SST (without annual cycle) was significant are shown in (E).

region can be explained by the annual cycle, and therefore it is somewhat predictable. Two areas on the coast of Chiloé island stood out as particularly cold: the southeastern section, south of the Desertores islands, and the northwestern section, west of the Chacao channel (Fig. 2A). Low mean temperatures and low STD in these areas are consistent with the small amplitude of the annual cycle, with 40–50 % of the variance in these areas unaccounted for by harmonic seasonal fluctuations (Fig. 2D). The climatological monthly averages (not shown here) showed that during the spring-summer months (September–February), these areas remain colder, which is reflected in the long-term average. The trend analysis showed significant increases in SST of ca. 0.25 °C per decade, especially in areas with overall warmer temperatures and larger amplitude in the annual cycle (Fig. 2E).

Atmospheric forcing in the region, which was characterized through calculations of coastal Ekman transport from CCMP wind fields, revealed a clear spatial-temporal pattern in terms of monthly climatology along the region of interest (Fig. 3). While downwelling favorable transport were observed year-round south of 46° S, there is a marked seasonality north of this latitude, especially off Chiloé Island, with offshore Ekman transport (i.e., upwelling favorable winds) from November to April (austral spring-summer) and onshore transport (i.e., downwelling favorable winds) from May to October (austral fall-winter). Also, the coastal Ekman climatology revealed that during austral spring-summer Chiloé Island is located in the transition between upwelling-favorable and downwelling-favorable winds (Fig. 3).

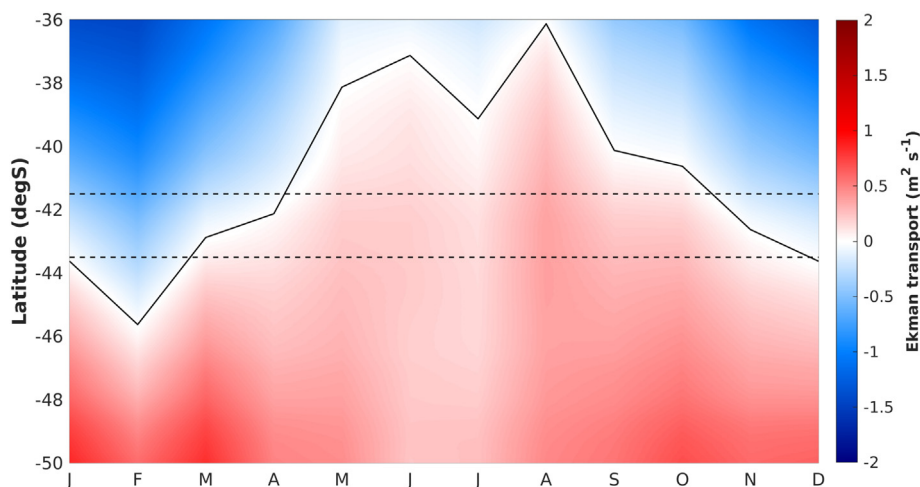


Fig. 3. Climatology of coastal Ekman transport along 75.25° W in south-central Chile estimated from CCMP Reanalysis v2 wind fields with 0.25° of resolution. The black contours represent the transition between upwelling (blue) and downwelling (red) favorable winds. Dotted horizontal lines indicate the northern and southern boundaries of the study area (i.e., Chacao channel and Guafo mouth).

3.2. Large- to meso-scale variability

Hovmöller plots of satellite SST anomaly time series over the 2003–2018 period along the western (Fig. 4A) and eastern (Fig. 4B) shores of the Chiloé Island showed a coherent temporal and spatial pattern, with damped variability in the ISC. Absolute temperature anomalies were generally higher along the western shore (Fig. 4A,B). Positive anomalies were predominant during 2003–2007, 2008–2009 and more intense in 2015–2017. The period with positive anomalies in 2008–2009 interrupted an otherwise long period of negative anomalies from 2007 to 2014. Along the region, coastal Ekman transport during 2003–2018 exhibited strong seasonality and interannual variability in both the duration and latitudinal extent of upwelling favorable conditions (Fig. 5A). The seasonal variability closely follows the climatology described before (Fig. 3), but there are marked differences among years. For instance, the upwelling season in 2007, 2008, and 2016 appeared to be longer and to extend farther south than other years. The analysis of interannual patterns in summertime Ekman transport (i.e., averaged for December–March) revealed a southward displacement of the transition between upwelling and downwelling favorable winds. The latitude of transition between predominant upwelling- and downwelling-favorable winds in summer months showed a significant trend ($p < 0.05$) to move southward at a rate equivalent to ca. 0.11° (~11.1 km) per year (Fig. 5B).

The temporal variability of meridionally-averaged SST anomalies on both sides of the Chiloé Island appeared to be associated with climate variability in the Pacific Ocean (Fig. 6). The SST anomalies on both shores of Chiloé Island roughly followed the Multivariate El Niño Index

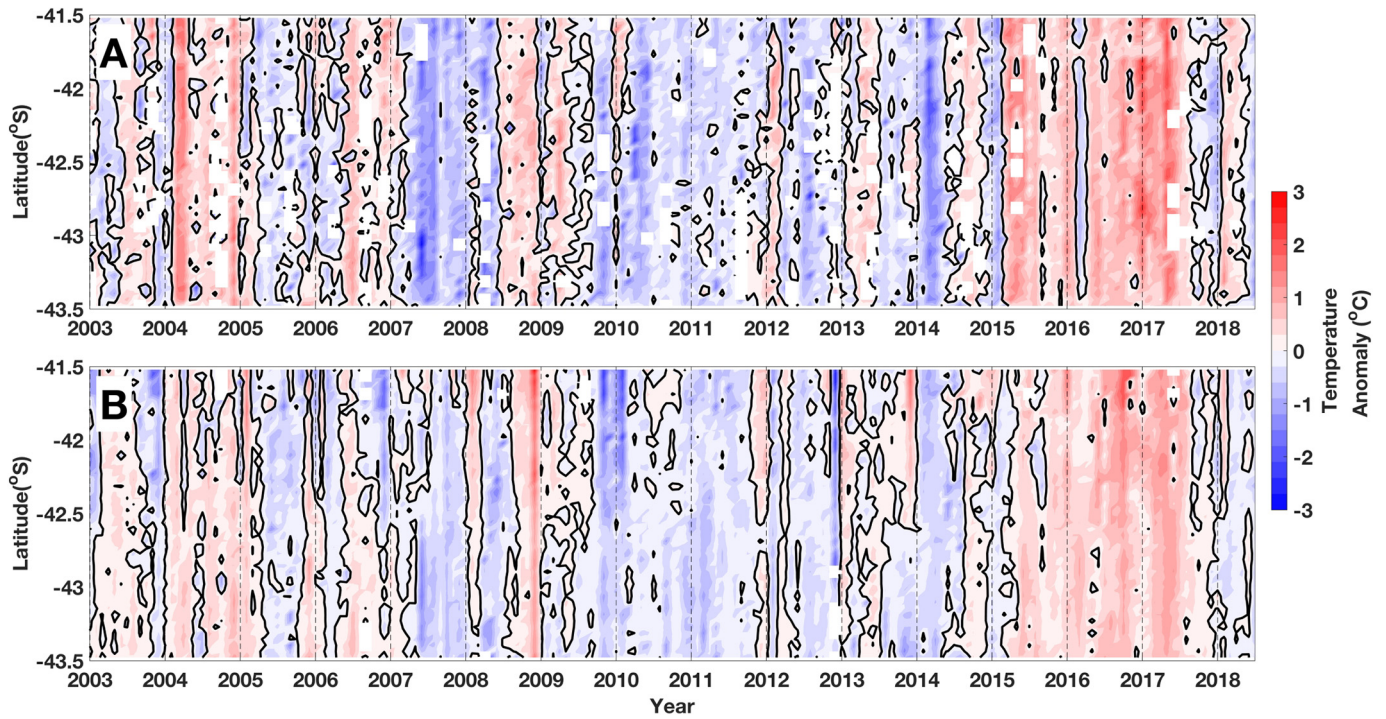


Fig. 4. Hovmöller plots showing Sea Surface Temperature (SST) anomalies along the western (A) and eastern (B) shore of the Chiloé Island. Black contours represent the zero anomaly.

(MEI) and the Pacific Decadal Oscillation (PDO). Periods with positive MEI and SST anomalies seemed to be associated to El Niño years (red dots in Fig. 6A) and negative SST anomalies appeared to be related to La Niña years (blue dots in Fig. 6A). Cross correlation between the MEI and SST-anomaly showed significant correlations at negative lags of 4–5 months ($r = 0.5$, $p < 0.05$) and at positive lags of 0–5 months ($r > 0.3$, $p < 0.05$). Protracted episodes of positive SST anomalies (extending for ca. 2 years) at the beginning (2003–2005) and end (2014–2017) of the time series matched positive phases of the MEI

(Fig. 6B) and the PDO (Fig. 6C). There was also a match between the 2007–2015 negative SST anomalies and a negative phase of the MEI, also associated with negative PDO. Significant correlations ($r = 0.36$ – 0.44 , $p < 0.05$) at time lags of -12 and $+12$ months were found between SST anomalies and the PDO. The 2008–2009 and 2010–2011 periods when positive SST anomalies occurred during negative phases of the MEI and PDO, seemed to be an exception to the otherwise good agreement between SST anomalies and the MEI/PDO phases. These exceptions also occurred during a period when the westerlies were

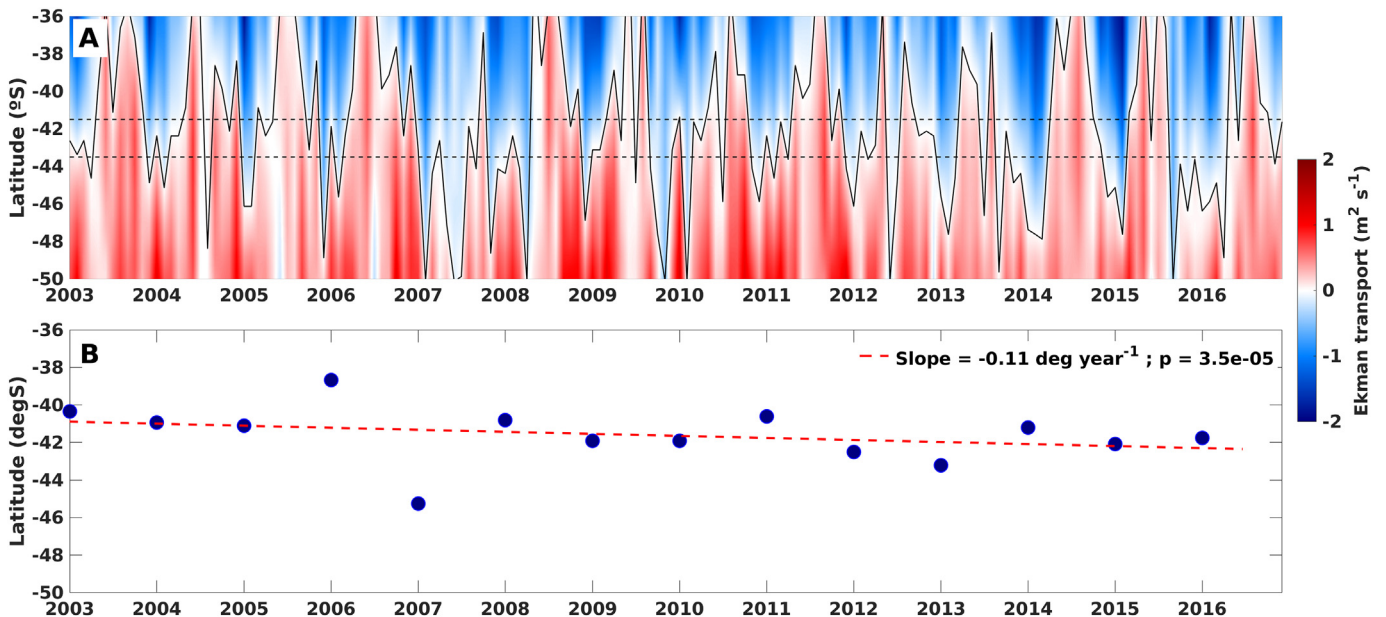


Fig. 5. Hovmöller plots showing monthly coastal Ekman transport along 36–50° S, estimated from wind data produced by CCMP Reanalysis v2 at 75° W (every 0.25°) (A). Blue and red coloring correspond to upwelling and downwelling favorable winds, respectively. The black contour corresponds to the transition between upwelling and downwelling. The bottom panel shows the summer-averaged latitudinal position of the upwelling-downwelling transition (B). A linear trend analysis indicated a significant slope of ~ -0.11 /year, i.e., poleward displacement of 11 km/year.

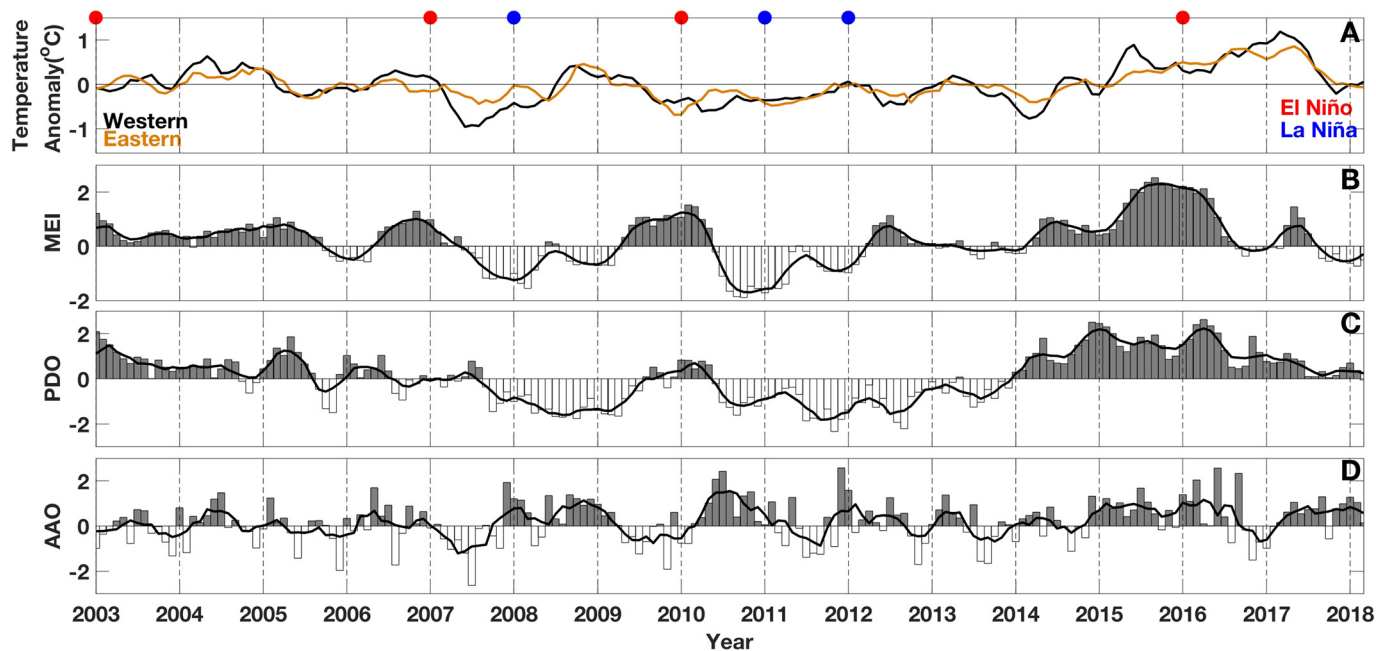


Fig. 6. Time series of monthly meridional means for SST anomalies (see Fig. 4) on the western (black) and eastern (orange) shore of Chiloé Island (A), monthly MEI (B), monthly PDO (C), and monthly AAO (D) climate indices. Gray and white bars in B–D represent positive and negative anomalies, respectively. Lines in (A) and the solid black line on top of bars in (B–D) correspond to 5-month running averages. El Niño and La Niña years, according to NOAA's Earth System Research Laboratory (https://www.esrl.noaa.gov/psd/enso/past_events.html), are indicated by red and blue dots on the top panel.

displaced polewards, i.e., positive AAO (Fig. 6D). This condition could also explain warmer waters in the Chiloé region, although the correlation found between SST and AAO was weak ($r = 0.24$, lag = +4 months, $p < 0.05$).

3.3. Local variability

To connect the mesoscale variability with local conditions amid the complex geographic setting of the ISC, we compared SST satellite data to *in situ* temperature data collected by the PSMB at multiple locations, as well as with data collected at Puerto Montt (see Fig. 1 for locations). Monthly averaged PSMB temperatures captured seasonal variability and a damped seasonal cycle during 2009–2010, which was also observed in the monthly satellite SST as well as in Puerto Montt *in situ* data (Fig. 7A). Satellite and PSMB temperature anomalies showed significant correlations ($r = 0.8$, $p < 0.05$) and overall synchronous fluctuations (Fig. 7B). Similar variability was observed at Puerto Montt, suggesting that these local measurements reproduce correctly the temporal variability in surface temperature along the ISC. Data from the PSMB are collected across a broad range of bathymetric and topographic conditions, and local differences in temperature seemed to reflect this heterogeneity, especially during summer months. Despite this heterogeneity, however, periods with higher temperatures were coherent along most of the region (Fig. 7C).

Time series from the 2 coastal moorings deployed in the ISC (see Fig. 1) allowed us to further examine the local variability along a 2-year record of physical, biological and chemical variables (Fig. 8). Seasonal variability was evident for all the variables recorded, although with some differences between locations. Warm temperatures were observed during the austral spring-summer (November through April), with water temperature at Quiquel up to 2° C warmer than at Vilupulli (Fig. 8A). The summer of 2015–2016 was slightly warmer than 2016–2017 at both locations, following the 2016 El Niño event. There was marked intraseasonal (~30 days) variability during the 2015–2016 spring-summer season. While temperature raised following the seasonal increase in solar radiation, there were 4 big drops in temperature at the end of November, December, January and February (Fig. 8A). These

temperature drops were sharper at Quiquel than at Vilupulli. The surface temperature at Puerto Montt, approximately 120 km north of these local moorings, was warmer on average but showed similar variability.

To verify whether the drops in temperature responded to fortnightly tides, satellite SST averages during spring and neap tides were estimated (Fig. 9). Spring tides might decrease the surface temperature by strong vertical mixing by tidal currents, thus, drops in SST at the same tidal frequency can be attributed to the tidal forcing. The estimated averages showed a similar pattern in both spring (Fig. 9A) and neap (Fig. 9B) tides. The differences between both averaged SST fields showed a more heterogeneous distribution, but only at Desertoires Island and around some localized coastal areas, the SST during neap tide were warmer than SST during spring tide (Fig. 9C), as it might be expected by fortnightly tidal forcing. Specifically around Quiquel, Vilupulli and Puerto Montt, the SST during spring tide was warmer than during neap tide, indicating that the drops in temperature were more likely caused for another forcing. Comparisons between the time series at the coastal moorings with the occurrence of spring tide (black triangles in Fig. 8A) also shows little correspondence of fortnightly tides and surface temperature.

Salinity at Quiquel was lower than at Vilupulli, but at both locations salinity showed an increasing trend from September 2015 to July 2016, with salinity increasing by ~1 over 10 months (Fig. 8B). Consistent with this increase in salinity, monthly precipitation exhibited a decreasing trend. Overall, 2016 was drier than 2015, which may explain interannual differences in salinity (supplementary figures, Fig. S2). Quiquel exhibited the same 30 day pattern of variability during the 2015–2016 summer season, where drops in temperature seemed to be coupled with increases in salinity (Fig. 8B). The highest chlorophyll concentrations were recorded at both sites during the spring-summer season (Fig. 8C). While chlorophyll concentration at Vilupulli exhibited larger peaks in 2015–2016, higher values were observed at Quiquel during the 2016–2017 season. Apparently, the 30 day periodicity in chlorophyll concentration at Vilupulli was linked to increases in temperature. The austral summer season also presented more variable dissolved oxygen (DO) in both locations, with slightly higher DO at Quiquel (Fig. 8D). The 30 day pattern of variability was detected for DO

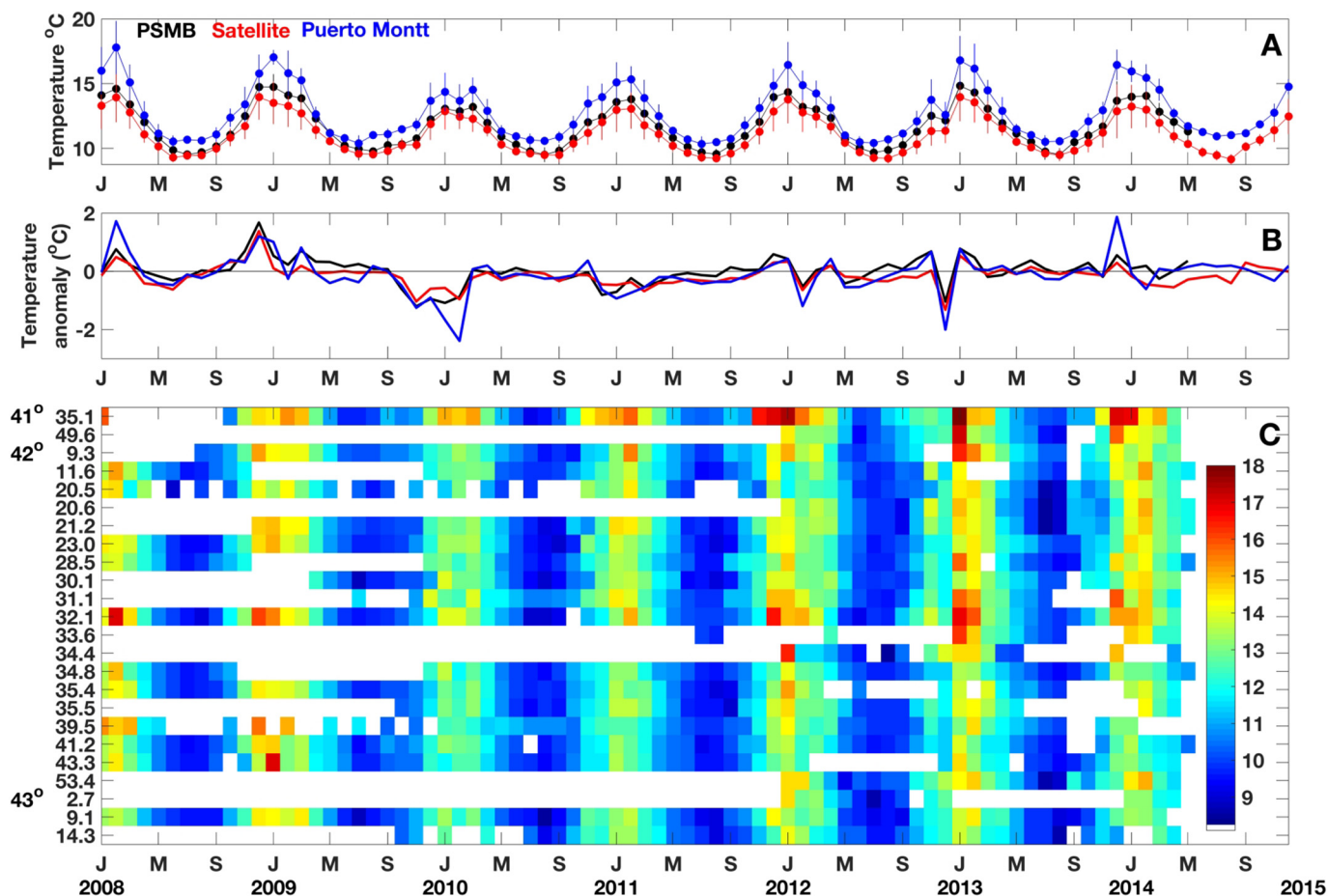


Fig. 7. Comparison between SST data from satellite, PSMB and Puerto Montt *in situ* records. Monthly- and meridionally-averaged temperature (A) and anomaly (B). The error bars represent ± 1 standard deviation. The bottom panel is the monthly-averaged PSMB temperature for each locality (C), represented by its latitude (degree and minute) in the y-axis.

at both locations, with changes of 2 ml L^{-1} . Both sites exhibited high variability in pH levels during the austral summer season, with higher pH at Quiquel (except for December 2015). Low pH conditions were observed during winter months, ranging from 7.6 to 7.9 pH units (Fig. 8E). Variability in pH was significantly correlated with DO concentration (Vilupulli: $r = 0.97$, $p < 0.01$; Quiquel: $r = 0.95$, $p < 0.01$) and its intraseasonal pattern. Collection of water samples for pH measurements and data validation from the SeaFET sensor indicated that observed pH was well correlated with monthly *in situ* pH estimates (supplementary figures, Fig. S3). Nevertheless, high pH conditions were also observed during high-chlorophyll periods. Although the sensor arrays were located at 4 m depth, the CTD profiles taken when the moorings were serviced showed a relatively well mixed water column in austral winter, and with a weak temperature and salinity stratification in the austral spring-summer seasons (supplementary figures, Fig. S4). Thus, the patterns of temporal variability observed at these moorings can be representative of the entire water column.

Spectral analysis showed that periods of ~ 14 and ~ 30 days were predominant in the time series (Fig. 10). For Vilupulli, the 30 day period was less apparent in the chlorophyll and salinity records (Fig. 10A) while for Quiquel the 14-day period was only evident in the chlorophyll records (Fig. 10B). To corroborate the previous results and further explore the main variability, we performed a wavelets analysis on the longer time series of SST and sea level recorded at Puerto Montt (Fig. 11). The data series were band-pass filtered, to focus the analysis on synoptic and intraseasonal fluctuations, i.e., between 5 and 100 days. The SST wavelet showed a consistent dominance of 8–60 day periods in the spring-summer season (Fig. 11A), with the 30–60 day

fluctuations spanning a longer time interval than shorter periods (8–16 days). Fluctuations in the 30–60 day band were absent only during the 2014–2015 season. For the 2015–2016 season, there was significant variability with periods centered at ~ 30 days (Fig. 11A), consistent with the peak found in the spectral analysis of the moorings time series (Fig. 10). The time-averaged SST spectrum (global power spectra) (Fig. 11B) showed the most significant variability in the intraseasonal scale, i.e., 30–90 days. The sea level wavelet spectra showed a significant band centered on periods of 15 days (Fig. 11C), with episodic fluctuations in the 60-day band that were not significant in the global power spectra (Fig. 11D). The band of 30–60 days was clearly observed in the Madden Julian Oscillation index (Fig. 11E,F), and it was consistent throughout the time series, with the exception of 2007 and 2010–2011. The wavelet coherence spectra (not shown) did not indicate significant relationships between the data series at any of the significant periods shown before.

3.4. Between-site relationships

We observed significant between-site correlations for water temperature ($r = 0.9$, $p < 0.05$), salinity ($r = 0.7$, $p < 0.05$), and dissolved oxygen ($r = 0.7$, $p < 0.05$), which suggests that local variability was forced by similar oceanographic processes. For each location, the analysis of cross-correlations between the observed variables showed significant positive correlations at time lags of 60–90 days (not shown). Correlations at 0 lag showed that temperature was positively correlated with salinity, oxygen (except at Vilupulli), and chlorophyll, i.e., an increase/decrease in temperature was coupled to a increase/decrease in

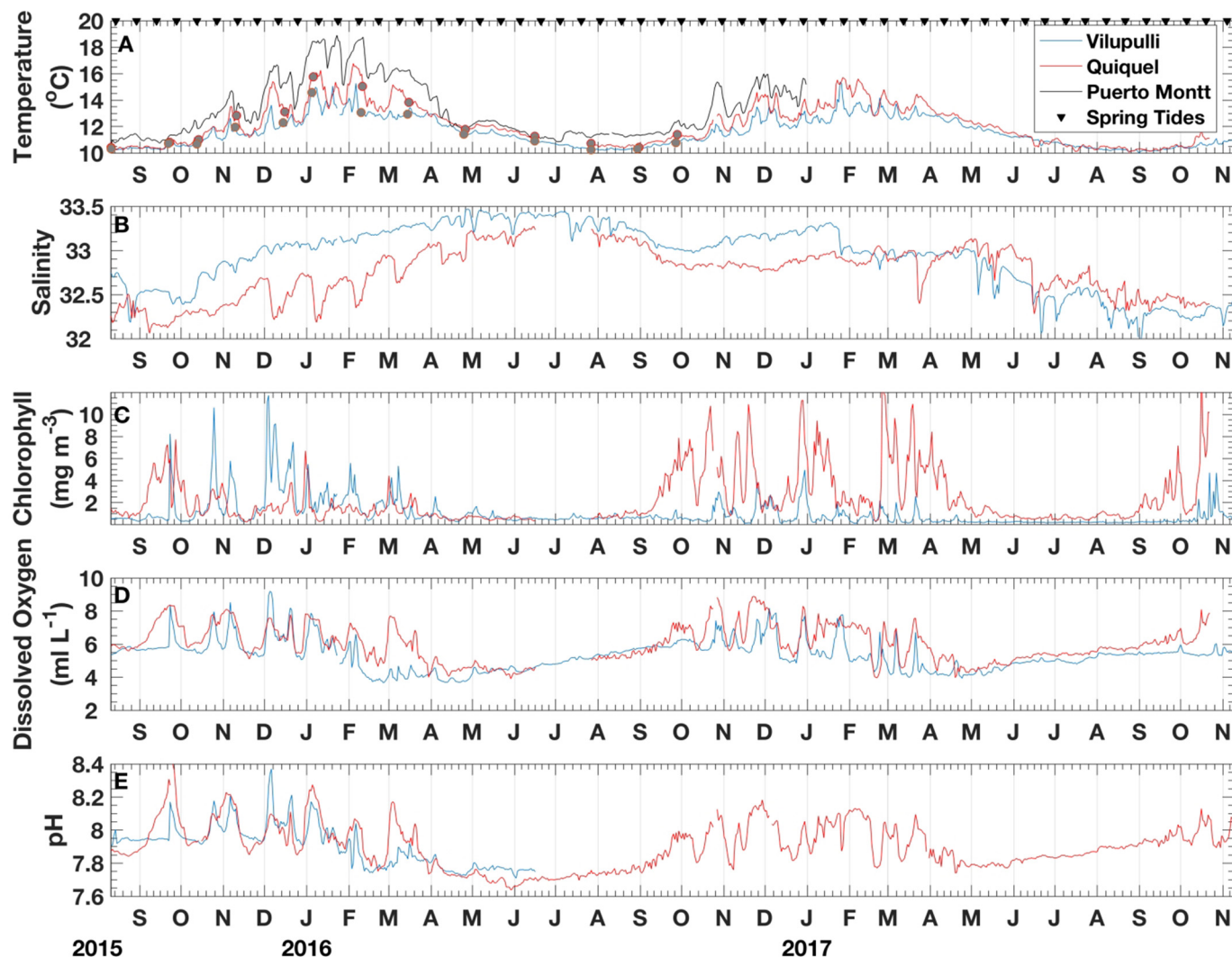


Fig. 8. Time series of daily-averaged temperature (A), salinity (B), chlorophyll (C), dissolved oxygen (D) and pH (E) recorded at 4 m depth at two locations in the eastern Chiloé Island: Vilupulli (South) and Quiquel (North). Black triangles on the top panel show the dates of spring tides. Gray dots indicate dates when CTD casts were performed (see Fig. S4, supplementary figures).

salinity, oxygen, and chlorophyll (Table 1). Salinity was negatively correlated with oxygen and chlorophyll (with the exception of Vilupulli), whereas oxygen and chlorophyll were positively correlated (Table 1).

4. Discussion

Our analyses revealed that patterns of atmospheric and oceanographic variability across the ISC region are highly heterogeneous both in time and space. The latitudinal position and topographic complexity of the coastline make this region particularly sensitive to inter-annual changes in environmental forcing (e.g., Iriarte et al., 2014; Garreaud et al., 2013), whereas region-wide evidence of anthropogenic forcing in recent times seems to be more equivocal. Considering that this region constitutes one of the most important areas for both salmon and shellfish aquaculture in Chile, it is critical to establish the various mechanisms, from local to regional scale, through which variability in physical (SST, wind, salinity) and biogeochemical (chlorophyll-a, oxygen, pH) conditions may impact such a relevant socio-economic activity in the region.

4.1. Large- to meso-scale variability

Overall, the climatic conditions of this region are characterized by a seasonal cycle in atmospheric forcing that is subject to important inter-annual variability (e.g., Garreaud and Falvey, 2009; Garreaud et al., 2013). CCMP wind data for the ocean region off the ISC revealed a climatological pattern where upwelling-favorable winds are observed during late spring and early summer chiefly in the northern sector (Fig. 3), with substantial interannual differences in the spatial-temporal pattern of Ekman transport for the region (Fig. 5). Our results not only confirm previous studies by Garreaud and Falvey (2009) and Garreaud et al. (2013), but also provide new information about the spatial-temporal scale in which the upwelling-downwelling transition might occur along this region. Although the transition extends over most of northern Patagonia, it is centered around the Guafo Mouth (Fig. 5A), which is the main connection and way of water exchange between the ISC and the adjacent continental shelf. Consequently, the ISC appears to respond rapidly to the mesoscale variability driven by open-ocean winds off southern Chile.

Part of the variability observed in SST is driven by the seasonal cycle in solar radiation, with substantial heterogeneity over this region due to variability in cloud cover at mesoscale as well as local scale. In addition to the warmer climatological mean temperature for the northern ISC

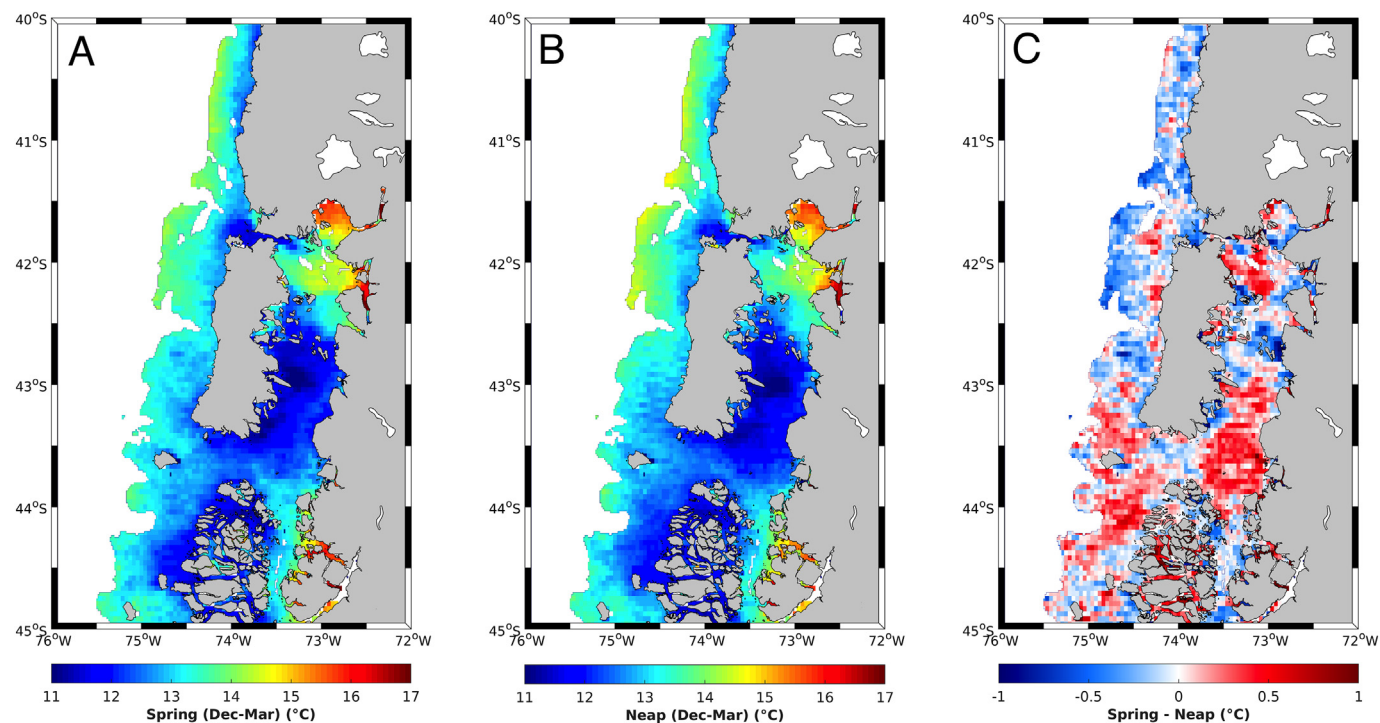


Fig. 9. Daily Aqua-MODIS SST averaged for spring (A) and neap (B) tides. Panel C shows the difference between spring tide and neap tide averages, with blue shades indicating that SST during spring tides is colder than during neap tides. The figure shows only depths < 300 m to focus on areas where topography and tides interaction can be expected.

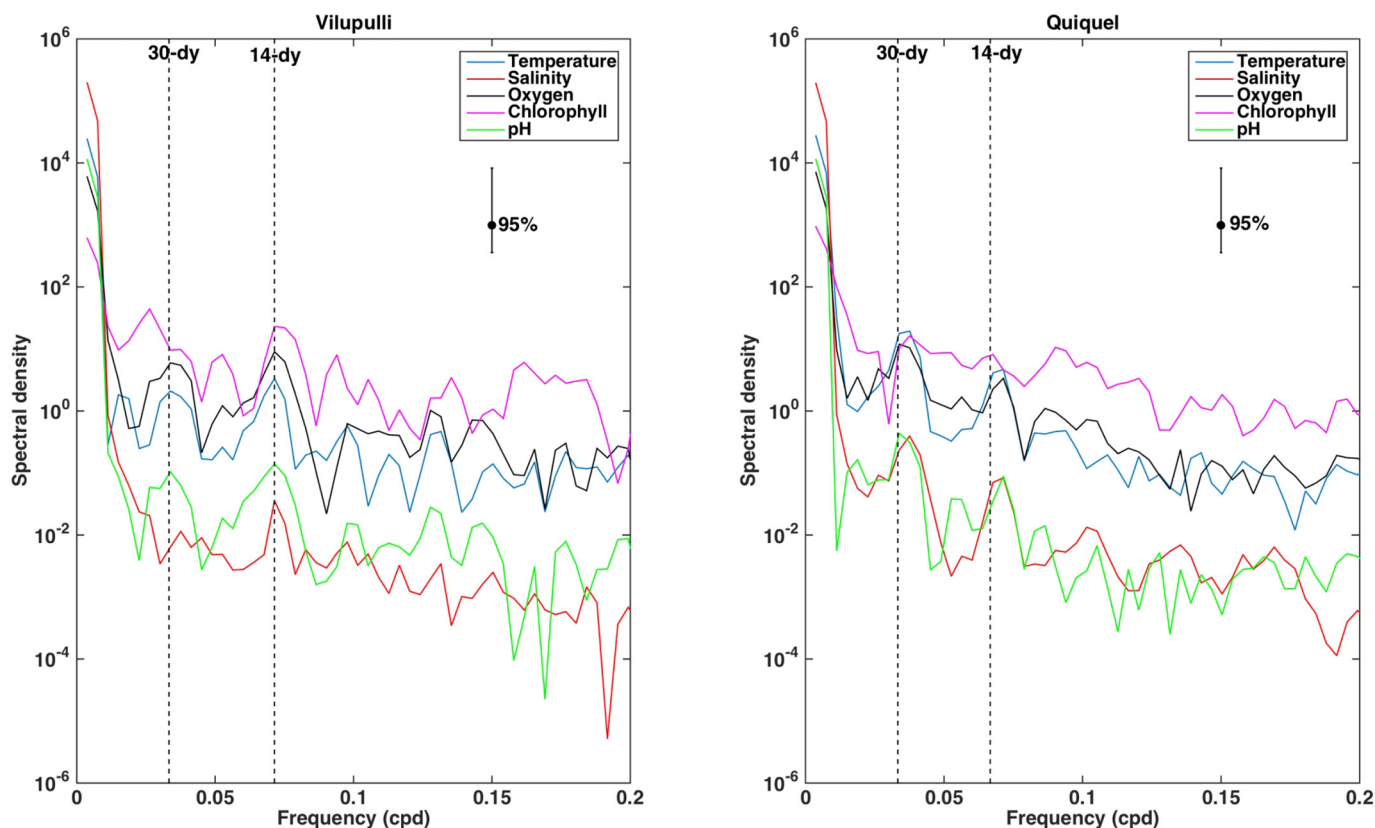


Fig. 10. Power spectra for all time series collected at the two monitoring sites on the eastern Chiloé Island: Vilupulli (South) (A) and Quiquel (North) (B).

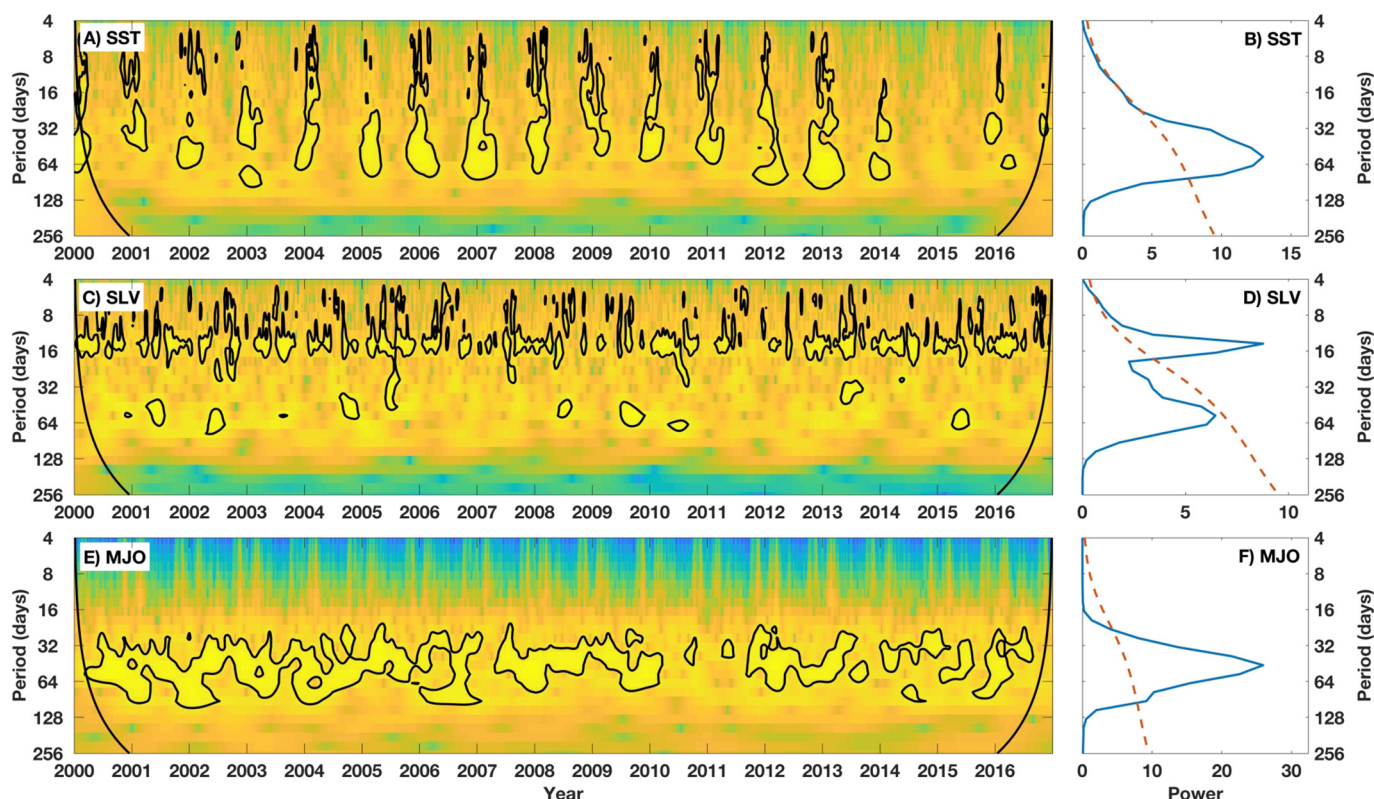


Fig. 11. Wavelets analysis for the band-pass filtered time series of sea surface temperature (SST) (A) and sea level (SLV) in Puerto Montt (C); and for the first EOF of the Madden Julian Oscillation Index (E). The cone of influence is shown by the black lines. Power values inside black contours are significant at 95 %. Right panels are the corresponding time-average over all time (global) wavelet power spectra (B, D and F).

Table 1

Correlation coefficients computed for all combinations of temperature (Temp), salinity (Sali), dissolved oxygen (Oxyg), and chlorophyll-a (Chla) measured at the southern and northern moorings on the eastern shore of Chiloé. Significant correlations are shown in boldface. * = $p < 0.05$; ** = $p < 0.01$; *** $p < 0.001$.

Pair	Southern mooring (Vilupulli)	Northern mooring (Quiquel)
Temp vs. Sali	0.43 ***	0.16 **
Temp vs. Oxyg	0.03	0.29 ***
Temp vs. Chla	0.34 ***	0.16 ***
Sali vs. Oxyg	-0.19 ***	0.50 ***
Sali vs. Chla	0.13 **	-0.05
Oxyg vs. Chla	0.53 ***	0.55 ***

and Reloncaví Sound, consistent with previous findings by Lara et al. (2016), we have shown a weak but significant warming trend in these and some other sections of the region, with rates of increase of ca. 0.1–0.25 °C per decade (Fig. 2E). Two areas that are persistently cold were identified: outside the Chacao channel and the southeastern shore of Chiloé Island. In both areas, a much smaller fraction of total SST variance was explained by the annual harmonic (Fig. 2D), suggesting that other processes are strongly modulating local circulation and residence times, and attenuating the development of a stronger seasonal signal in SST. The process driving the strong gradient of SST along the ISC, with warm water in the northern section and colder water in the south, is still unclear. However, our finding of a larger amplitude in the annual SST cycle on the northern section of the ISC suggests that differences in the residence times of surface waters, combined with wind and/or tides may explain this gradient. The presence of topographic features such as the Desertores islands and the narrow Chacao channel, together with a change in bathymetry, might reduce current velocities and dampen wind influence on surface mixing in the northern section of

the ISC, thus allowing greater warming of surface waters.

Although the temporal resolution of available data limits our analysis to subtidal variability, we addressed the issue of potential cooling by fortnightly tidal mixing using the SST satellite images (Fig. 9). In estuarine environments, stronger mixing occurs during spring tides and, therefore, surface warming is expected to be attenuated relative to neap tides (Valle-Levinson and Wong, 2000; MacCready and Geyer, 2010; Iwasaki et al., 2015). Although our results are not conclusive, areas with bathymetric constraints where stronger tidal currents are expected (e.g., Desertores islands), colder temperature were in fact detected during spring tides. This spring/neap tide difference in SST was not apparent for areas that appeared colder in the climatology, namely the western end of the Chacao channel and the southeastern shore of Chiloé island. We hypothesize that wind mixing has as much - or more - influence on the cooling of surface waters at these sites than tide-driven mixing in the spring-summer months. Understanding the processes driving vertical mixing and residence times in the ISC is key to identify bottom-up controls of its primary and secondary productivity, especially considering the importance of this region's productivity for aquaculture, as well as for the seasonal feeding of large whales (Hucke-Gaete et al., 2010, 2004; Buchan and Quiñones, 2016).

Together with the finding of a significant poleward displacement in the latitudinal transition from upwelling-favorable to downwelling-favorable winds during summer months, we documented the connection between large-scale climatic forcing and variability in surface conditions across the region, as revealed by the satellite-derived time series and their correlation with large-scale climate indices. For example, the 2015–2016 ENSO event had a clear impact on SST around the region. In general, satellite-derived SST anomalies were in good agreement with variability in the MEI, PDO and AAO, except for some inconsistencies in the timing and duration of anomalies. Our analyses show that ENSO conditions have a 4–5 month lead over anomalous temperature conditions in the ISC. However, positive phases of both PDO and AAO also

co-occur with a positive MEI; thus, ENSO events might not be the main driver of the inter-annual SST anomalies. A connection between ENSO and changes in the abundance of larval mussels in the northern ISC has been previously reported (Lara et al., 2016), suggesting a link between large-scale processes and the coupling of physical and biological processes at local scale. Equatorial influence is mediated by low latitude conditions around the study area through the position and latitudinal extent of the westerlies, such as the pattern observed during the 2008–2009 period, where positive SST anomalies occurred during negative phases of the MEI and PDO. The AAO presents a meridional displacement related to variability of the westerlies (Spence et al., 2014). In the last decades the AAO has shifted to a positive phase, which has resulted in a strengthening of the westerlies (Marshall et al., 2006). The strength of the ENSO tele-connection to the South Pacific is the result of coupling between ENSO and the AAO (Fogt et al., 2011). Additionally, the South Pacific High (SPH), a subtropical anticyclone system located over the south Pacific, exhibits a seasonal displacement. During the austral winter, the SPH moves northward allowing frontal weather systems to reach central Chile (30–40° S), whereas during summer it moves southward, thus intensifying southerly upwelling-favorable winds in central and southern Chile (35–42° S) (Schneider et al., 2017). The SPH not only drives the seasonality of upwelling favorable winds along the Chilean coast. South of 42–43° S, it generates mostly downwelling-favorable winds (i.e., northerly winds). Hence, the recent presence of upwelling-favorable winds around the ISC (Fig. 5) may be part of a trend related to changes in the seasonal position of the SPH following the intensification of the westerlies.

4.2. Meso-scale to local variability

One outstanding temporal feature revealed by our analysis of *in situ* time series was the predominance of an intraseasonal band with periods of ~ 30 days for a range of variables - but more evident for water temperature - at both mooring locations. There is also large inter-annual variability of the intraseasonal fluctuations, i.e., they appear to be more energetic on some years. Such intraseasonal fluctuations can be associated to coastal trapped waves (CTW) (e.g., Shaffer et al., 1995; Hormazabal et al., 2001), atmospheric forcing caused by the Baroclinic Annular Mode (BAM) (Thompson and Woodworth, 2014; Ross et al., 2015) and Madden Julian Oscillations (MJO) (Gao and Stanford, 1988; Wang and Ding, 1992). The sum of the fortnightly tidal cycle (spring-neap tides) might also introduce a distortion with periodicity close to 30 days. The sea level wavelets clearly showed the predominance of fortnightly tides in the records, with less influence of variability associated to CTWs (see Fig. 10C,D). To our knowledge, CTWs have not been reported for the ISC, and our analysis of sea level records showed only weak variability at the time scale that corresponds to CTWs. The resonance of diurnal and semidiurnal tides detected for the ISC (e.g., Aiken, 2008) might mask the CTW signal. However, the width of the Guafo Mouth (40 km) is smaller than the Rossby ratio of deformation (~300 km, $h = 100$ m), thus precluding the propagation of progressive waves inside the ISC. The MJO drives atmospheric fluctuations with periodicity around 45 days, propagating from the equatorial Indian Ocean to southern South America (40° S) and back to the Indian Ocean through southern Africa (Gao and Stanford, 1988). Thus, the 30 day periodicity observed in our results seems to be more consistent with periodicity shorter than MJO, such as the variability scales found for the Baroclinic Annular Modes (BAM). This result highlights the effects of Southern Hemisphere climatic variability (Thompson and Woodworth, 2014) on coastal waters of western Patagonia. Recently, BAM effects on the intraseasonal variability of local circulation in a Patagonian fjord were documented by Ross et al. (2015). Winds associated to extreme low-pressure systems were shown to alter the pycnocline, thermal structure and circulation in a fjord 500 km south of our study area (Ross et al., 2015). Our work confirms that the influence of this atmospheric phenomenon on local mixing and biogeochemical

conditions may span an important section of the Chilean Patagonia. For example, pH was highly correlated with DO and its intraseasonal variability, following the linkage between photosynthesis and respiration, suggesting that remote forcing can modulate the strength of key biogeochemical processes. Although the relationship between pH and freshwater input through precipitation and river discharges can be important (e.g., Pérez et al., 2015), typically, in coastal regions the pH conditions can be controlled by the balance between photosynthesis (Chl-a) and respiration (O_2) (Torres et al., 2011; Vargas et al., 2017), which explains not only the significant correlation with DO, but also the high pH conditions during phytoplankton blooms (inferred from high-chlorophyll events). Given the short time scale of the pH time series, it is difficult to estimate a long-term trend that can be associated to ocean acidification. Typically, the time of emergence (defined as the point in time when the trend exceeds two times the pH background natural variability) can be longer than 10 or 20 years, which is 3 times longer than the time of emergence of more stable open ocean pH conditions (Keller et al., 2014; Kapsenberg and Hofmann, 2016). Therefore, longer pH time series are needed to evaluate more definitively the effects of ocean acidification in this area. Nevertheless, datasets such as those presented here provide valuable baseline information to establish the natural variability of pH, which is useful for making projections and designing experimental work with coastal marine organisms.

4.3. Implications for aquaculture sustainability and future environmental change

The coastal ocean sustains a large fraction of the fisheries and aquaculture production worldwide, and the ISC region is an exceptional example, as it accounts for the bulk of the farmed salmon and shellfish exported by Chile, which has been ranked among the top five global marine seafood producers over the past decade (FAO, 2016). However, this region is increasingly affected by environmental events related both to climatic and human-induced variability. For example, inter-annual variability driven by the type of large-scale forcing described above seems to have played a role in the collapse of seed supply to the mussel aquaculture during the 2010–2012 period (Lara et al., 2016). On the other hand, short-term crises like the outbreak of the Infectious Salmon Anemia Virus (ISAV) during mid-2007, which lowered the salmon production by 30 %, was driven by breaches to food-production sanitary protocols (Smith et al., 2010). Furthermore, harmful algal blooms (HABs) have been detected in western Patagonia occasionally since 2002 (Fuentes et al., 2006) and a recent event, related to the proliferation of the dinoflagellate *Alexandrium catenella* after an anomalously warm and calm summer resulted in the loss of 1800 metric tons of farmed salmon (León-Muñoz et al., 2018; Mardones et al., 2016). Although HABs do not directly affect the shellfish production, the prohibition of seafood consumption mandated by the Chilean Health Department during these events implies large losses for the aquaculture and tourism industry. On the other hand, little is known of the potential damages to fjord ecosystems imposed by a substantial increase in the use of fjords by aquaculture, especially the response to sustained drops in dissolved oxygen below critical levels, as well as increases in nutrient concentrations. Our comparisons between satellite and *in situ* temperature data collected in the framework of the mandatory environmental monitoring programs (Fig. 7) indicate that PSMB temperature records are reliable despite the caveats we outlined for this monitoring program. Hence, the use of collaborative sampling schemes coupled with the acquisition of data from remote sensing platforms and other emerging technologies offers some promise towards the sustainable use and management of the Chilean Patagonia coastal ecosystems.

Our analyses indicate an important trend in offshore conditions following our observation of a poleward displacement of upwelling-favorable conditions in reanalysis data, which is in agreement with recent modeling and observational evidence (Sydeman et al., 2014; Rykaczewski et al., 2015). The influx of upwelling water into the basin

may cascade into changes in nutrient availability and their relative concentrations, which combined with altered regimes of precipitation and runoff can translate into changes in phytoplankton composition (Iriarte et al., 2017; Ryan et al., 2017; Jacob et al., 2018). Additionally, an increasing prevalence of upwelling-favorable conditions could also increase the frequency of intrusions of low-oxygen Equatorial Subsurface Waters (ESSW) into the ISC and northern Patagonia fjords. Although currently there is no published work on the actual impact that coastal upwelling may have inside the fjords, our results show its frequent occurrence along the northern Patagonia coast during austral summer. More studies are required to ascertain the potential consequences of such a shift for the ISC ecosystem productivity and the economic activities that depend on it.

We have shown that patterns of mesoscale variability are tightly coupled with climatic indices (MEI, PDO and AAO), which provides a predictability lead over local conditions. It must be noted, however, that intraseasonal variability associated to the BAM might be a potential key modifier of local biogeochemical processes and subject to large changes over interannual scales in the southern Patagonia region (see Fig. 8). Finally, physical conditions in the ISC region are extremely heterogeneous, with areas subject to strong seasonal cycles, while other areas appear dominated by higher frequency variability from sources such as tides and winds. Such heterogeneity induces a clear spatial structure in the aptitude of certain sub-regions for different uses (e.g., shellfish fishing, mussel farming, whale conservation). Future environmental change such as ocean acidification, deoxygenation and warming could impact parts of this semi-enclosed basin differently, thus increasing the challenges to sustainability management of the multiple activities and uses of the ISC. The high variability in DO, temperature, and pH over multiple time scales that we documented in this contribution may have significant implications for local adaptation of marine populations upon changing ocean conditions (Vargas et al., 2017), and warrants further research in order to assess the adaptive capacity of both the organisms and the economic activities that are based on them, such as the Chilean mussel farming industry.

5. Conclusions

Our analyses revealed that patterns of atmospheric and oceanographic variability along northern Patagonia (40–45° S) are highly heterogeneous both in time and space. The main conclusions can be summarized as follows:

- There are two persistently cold areas around Chiloé island, where seasonal variability is attenuated by local-scale mixing. Although the exact mechanisms (tides, wind, local topography) driving the mixing remain unknown, understanding the interannual variability provides insights on the bottom-up controls of primary and secondary productivity in a region that, besides its importance for aquaculture, appears to be a hot-spot for whale feeding.
- Hydrographic conditions in northern Patagonia are strongly affected by the interaction of large-scale processes at the scale of the South Pacific basin. The subtle but consistent poleward displacement of the transition between upwelling- and downwelling-favorable winds detected for the past decade revealed a southward shift of the upwelling favorable winds during the summer.
- The intraseasonal time scale was dominated by a band around 30 day periodicity that can be attributed to atmospheric variability driven by the Baroclinic Annular Mode (BAM). This finding suggests that the influence of this atmospheric phenomenon on local mixing and biogeochemical conditions may extend over an important section of the Patagonian fjord system.
- The response of local-scale conditions to large-scale variability, even in the small channels and bays, highlights the importance of large-scale processes for local aquaculture activities in the region (e.g., through the impact of changing chlorophyll-a, DO, pH and

temperature conditions) and must be taken into account in the management and planning of the aquaculture industry in the context of future climate scenarios.

Acknowledgments

This research was funded by Millennium Nucleus “Center for the Study of Multiple-drivers on Marine Socio-Ecological Systems (MUSELS)” funded by MINECON NC120086. DAN acknowledges partial support from FONDECYT 11161091. Partial support for DAN and FJT was provided by COPAS Sur-Austral CONICYT PIA APOYO CTE AFB170006. Partial support for FJT was also provided by INCAR (FONDAP grant 15110027, CONICYT). CAV was also supported by Instituto Milenio de Oceanografía (IMO), MINECON IC120019.

Appendix A. Calibration of pH measurements

Measurements from the SeaFET pH (ISFET pH sensor) were corrected by temperature (both recorded by the WQM) using the equations from Martz et al. (2010). This correction indicated differences no greater than 10^{-13} between corrected and uncorrected pH data. The SeaFET pH data were also validated against *in situ* measurements collected monthly when servicing the sensors. Water samples were collected from the same depth where SeaFET sensors were deployed (4 m). Samples for SeaFET data validation were collected using a 5-l Niskin bottle, following Standard Operating Procedures (Dickson et al., 2007). Samples were transported to the laboratory within less than 2 h and transferred to a 25 ml thermostatted cell at $25.0 \pm 0.1^\circ \text{C}$ for standardization. Measurements were conducted on the total scale (pH_T) using a Metrohm 826 pH meter connected to a combined electrode LL Aquatrode plus Pt 1000, and calibrated using a Tris buffer at $25.0 \pm 0.1^\circ \text{C}$ ($\text{pH} = 8.089$).

Concurrently, Total Alkalinity samples were measured using an open-cell titrator (Dickson et al., 2007). *In situ* pH_T values were estimated using *in situ* data for temperature and salinity (from WQM located at the same depth), and calculated through the CO2SYS software for MS Excel (v2.2) with CO_2 constants from Lueker et al. (2000), KHSO_4 value from Dickson et al. (2007), and Total Boron value from Uppström (1974). The estimated error in pH analysis was < 0.003 pH units. Comparisons between *in situ* total pH and SeaFET pH were made by simple linear regression analysis. The WQM and SeaFET were set to measure every 20 s at the top of each hour. Prior to the deployment we performed sensitivity analysis considering measurement intervals of 10, 20 and 30 s. No significant changes were observed when decreasing or increasing the sampling interval.

Appendix B. Supplementary data

Supplementary data to this article can be found online at <https://doi.org/10.1016/j.jmarsys.2018.12.008>.

References

- Acha, E.M., Mianzan, H.W., Guerrero, R.A., Favero, M., Bava, J., 2004. Marine fronts at the continental shelves of austral South America: physical and ecological processes. *J. Mar. Syst.* 44, 83–105. <https://doi.org/10.1016/j.jmarsys.2003.09.005>.
- Aiken, C.M., 2008. Barotropic tides of the Chilean inland sea and their sensitivity to basin geometry. *J. Geophys. Res.* 113, C08024. <https://doi.org/10.1029/2007JC004593>.
- Buchan, S.J., Quiñones, R.A., 2016. First insights into the oceanographic characteristics of a blue whale feeding ground in northern Patagonia, Chile. *Mar. Ecol. Prog. Ser.* 554, 183–199. <https://doi.org/10.3354/meps11762>.
- Cáceres, M.A., Valle-Levinson, A., Atkinson, L.P., 2003. Observations of cross-channel structure of flow in an energetic tidal channel. *J. Geophys. Res.* 108, 1–10. <https://doi.org/10.1029/2001JC000968>.
- Castillo, M.L., Cifuentes, U., Pizarro, O., Djurfeldt, L., Cáceres, M., 2016. Seasonal hydrography and surface outflow in a fjord with a deep sill: the Reloncaví fjord, Chile. *Ocean Sci.* 12, 533–534. <https://doi.org/10.5194/os-12-533-2016>.
- Dávila, P.M., Figueroa, D., Müller, E., 2002. Freshwater input into the coastal ocean and its relation with the salinity distribution off austral Chile (35–55°S). *Cont. Shelf Res.*

- 22, 521–534.
- Dickson, A.G., Sabine, C.L., Christian, J.L., 2007. Guide to Best Practices for Ocean CO₂ Measurements. PICES Special Publication 3. North Pacific Marine Science Organization, Sidney, British Columbia.
- Emery, W.J., Thomson, R.E., 2001. Data Analysis Methods in Physical Oceanography. Elsevier Science, pp. 638.
- FAO, 2016. The State of World Fisheries and Aquaculture 2016. Contributing to Food Security and Nutrition for All. FAO, pp. 200.
- Fierro, J., Bravo, M., Castillo, M., 2000. Caracterización del régimen de mareas y corrientes a lo largo del canal moraleda (43°s-45°17's). Ciencia y Tecnología del Mar 3–14.
- Fogt, R.L., Bromwich, D.H., Hines, K.M., 2011, apr. Understanding the SAM influence on the South Pacific ENSO teleconnection. Clim. Dyn. 36, 1555–1576.
- Fuentes, C., Clement, A., Aguilera, A., 2006. Summer *Alexandrium catenella* bloom and the impact on fish farming, in the XI Aysen region, Chile. In: 12th International Conference on Harmful Algae. International Society for the Study of Harmful Algae (ISSHA), Copenhagen, Denmark.
- Gao, X.H., Stanford, J.L., 1988. Possible feedback path for low-frequency atmospheric oscillations. J. Atmos. Sci. 45, 1425–1432. [https://doi.org/10.1175/1520-0469\(1988\)045<1425:PFPLF>2.0.CO;2](https://doi.org/10.1175/1520-0469(1988)045<1425:PFPLF>2.0.CO;2).
- Garreaud, R.D., Falvey, M., 2009. The coastal winds off western subtropical South America in future climate scenarios. Int. J. Climatol. 29, 543–554. <https://doi.org/10.1002/joc.1716>.
- Garreaud, R.D., Lopez, P., Minvielle, M., Rojas, M., 2013. Large-scale control on the Patagonian climate. J. Clim. 26, 215–230. <https://doi.org/10.1175/JCLI-D-12-00001.1>.
- González, H.E., Castro, L.R., Daneri, G., Iriarte, J.L., Silva, N., Vargas, C.A., Giesecke, R., Sánchez, N., 2011. Seasonal plankton variability in Chilean Patagonia fjords: carbon flow through the pelagic food web of Aysen Fjord and plankton dynamics in the Moraleda Channel basin. Cont. Shelf Res. 31, 225–243. <https://doi.org/10.1016/j.csr.2010.08.010>.
- Hormazabal, S., Shaffer, G., Letelier, J., Ulloa, O., 2001. Local and remote forcing of sea surface temperature in the coastal upwelling system off Chile. J. Geophys. Res. Oceans 106, 16657–16671. <https://doi.org/10.1029/2001JC900008>.
- Hucke-Gaete, R., Álvarez, R., Navarro, M., Ruiz, J., Moro, P., Farías, A., 2010. Investigación para desarrollo de área marina costera protegida Chiloé - Palena - Guaitecas. Informe final de estudio financiado por FNDP - BID TURISMO N°30040215-0. Technical Report. Universidad Austral de Chile, Valdivia, Chile.
- Hucke-Gaete, R., Osman, L.P., Moreno, C.A., Findlay, K.P., Ljungblad, D.K., 2004. Discovery of a blue whale feeding and nursing ground in southern Chile. Proc. R. Soc. B Biol. Sci. 271, S170–S173. <https://doi.org/10.1098/rsbl.2003.0132>.
- Iriarte, J.L., González, H.E., Liu, K.K., Rivas, C., Valenzuela, C., 2007. Spatial and temporal variability of chlorophyll and primary productivity in surface waters of southern Chile (41.5–43°S). Estuar. Coast. Shelf Sci. 74, 471–480. <https://doi.org/10.1016/j.ecss.2007.05.015>.
- Iriarte, J.L., León-Muñoz, J., Marcé, R., Clément, A., Lara, C., 2017. Influence of seasonal freshwater streamflow regimes on phytoplankton blooms in a Patagonian fjord. N. Z. J. Mar. Freshw. Res. 51 (2), 30–315. <https://doi.org/10.1080/00288330.2016.1220955>.
- Iriarte, J.L., Pantoja, S., Daneri, G., 2014. Oceanographic processes in Chilean fjords of Patagonia: from small to large-scale studies. Prog. Oceanogr. 129, 1–7. <https://doi.org/10.1016/j.pocean.2014.10.004>.
- Iwasaki, S., Isobe, A., Miyao, Y., 2015. Fortnightly atmospheric tides forced by spring and neap tides in coastal waters. Sci. Rep. 5, 10167. <https://doi.org/10.1038/srep10167>.
- Jacob, B., Tapia, F.J., Daneri, G., Iriarte, J.L., Montero, P., Sobarzo, M.A., Quiñones, R.A., 2014. Springtime size-fractionated primary production across hydrographic and PAR-light gradients in Chilean Patagonia (41–50°S). Prog. Oceanogr. 129, 75–84. <https://doi.org/10.1016/j.pocean.2014.08.003>.
- Jacob, B.G., Tapia, F.J., Quiñones, R.A., Montes, R., Sobarzo, M., Schneider, W., Daneri, G., Morales, C.E., Montero, P., González, H.E., 2018. Major changes in diatom abundance, productivity, and net community metabolism in a windier and dryer coastal climate in the southern Humboldt Current. Prog. Oceanogr. 168, 196–209. <https://doi.org/10.1016/j.pocean.2018.10.001>.
- Kapsenberg, L., Hofmann, G., 2016. Ocean pH time-series and drivers of variability along the northern Channel Islands, California, USA. Limnol. Oceanogr. 61, 953–968.
- Keller, K., Joos, F., Raible, C., 2014. Time of emergence of trends in ocean biogeochemistry. Biogeosciences 11, 3647–3659. <https://doi.org/10.5194/bg-11-3647-2014>.
- Kraus, E., 1972. Atmosphere-Ocean Interaction. Oxford Univ Press, London UK.
- Lara, C., Saldías, G.S., Tapia, F.J., Iriarte, J.L., Broitman, B.R., 2016. Interannual variability in temporal patterns of Chlorophyll-a and their potential influence on the supply of mussel larvae to inner waters in northern Patagonia (41–44°S). J. Mar. Syst. 155, 11–18. <https://doi.org/10.1016/j.jmarsys.2015.10.010>.
- Large, W., Pond, S., 1981. Open ocean momentum flux measurements in moderate to strong winds. J. Phys. Oceanogr. 11, 324–336.
- León-Muñoz, J., Urbina, M.A., Garreaud, R., Iriarte, J.L., 2018. Hydroclimatic conditions trigger record harmful algal bloom in western Patagonia (summer 2016). Sci. Rep. 8, 1330. <https://doi.org/10.1038/s41598-018-19461-4>.
- Letelier, J., Soto-Mardones, L., Salinas, S., Osuna, P., López, D., Sepúlveda, H.H., Pinilla, E., Rodrigo, C., 2011. Variabilidad del viento, oleaje y corrientes en la región norte de los fiordos Patagónicos de Chile. Rev. Biol. Mar. Oceanogr. 46, 363–377.
- Lueker, T.J., Dickson, A.G., Keeling, C.D., 2000. Ocean pCO₂ calculated from dissolved inorganic carbon, alkalinity, and equations for K₁ and K₂: validation based on laboratory measurements of CO₂ in gas and seawater at equilibrium. Mar. Chem. 70, 105–119. [https://doi.org/10.1016/S0304-4203\(00\)00022-0](https://doi.org/10.1016/S0304-4203(00)00022-0).
- MacCready, P., Geyer, W.R., 2010. Advances in estuarine physics. Annu. Rev. Mar. Sci. 2, 35–58. <https://doi.org/10.1146/annurev-marine-120308-081015>.
- Mardones, J.L., Müller, M.N., Hallegraeff, G.M., 2016. Toxic dinoflagellate blooms of *Alexandrium catenella* in Chilean fjords: a resilient winner from climate change. ICES J. Mar. Sci. 74. <https://doi.org/10.1093/icesjms/fsw164>.
- Marshall, G.J., Orr, A., van Lipzig, N.P.M., King, J.C., 2006. The impact of a changing southern hemisphere annular mode on Antarctic Peninsula summer temperatures. J. Clim. 19, 5388–5404. <https://doi.org/10.1175/JCLI3844.1>.
- Martz, T.R., Connery, J.G., Johnson, K.S., 2010. Testing the Honeywell Durafet® for seawater pH applications. Limnol. Oceanogr. Methods 8, 172–184. <https://doi.org/10.4319/om.2010.8.172>.
- Nelson, C., 1977. Wind stress and wind-stress curl over the California current. Technical Report NMFS SSRF-71.
- Palma, S., Silva, N., 2004. Distribution of siphonophores, chaetognaths, euphausiids and oceanographic conditions in the fjords and channels of southern Chile. Deep-Sea Res. II Top. Stud. Oceanogr. 51, 513–535. <https://doi.org/10.1016/j.dsr2.2004.05.001>.
- Pantoja, S., Iriarte, J.L., Daneri, G., 2011. Oceanography of the Chilean Patagonia. Cont. Shelf Res. 31, 149–153. <https://doi.org/10.1016/j.csr.2010.10.013>.
- Pérez, C.A., DeGrandpre, M.D., Lagos, N.A., Saldías, G.S., Cascales, E.-K., Vargas, C.A., 2015. Influence of climate and land use in carbon biogeochemistry in lower reaches of rivers in central southern Chile: implications for the carbonate system in river-influenced rocky shore environments. J. Geophys. Res. Biogeosci. 120, 673–692. <https://doi.org/10.1002/2014JG002699>.
- Pérez-Santos, I., 2017. Deep ventilation event during fall and winter 2015 in the Puyuhuapi fjord (44.6°S). Lat. Am. J. Aquat. Res. 45, 223–227. <https://doi.org/10.3856/vol45-issue1-fulltext-25>.
- Ross, L., Valle-Levinson, A., Pérez-Santos, I., Tapia, F.J., Schneider, W., 2015, aug. Baroclinic annular variability of internal motions in a Patagonian fjord. J. Geophys. Res. Oceans 120, 5668–5685. <https://doi.org/10.1002/2014JC010669>.
- Ryan, J., Kudela, R., Birch, J., Blum, M., Bowers, H., Chavez, F., Doucette, G., Hayashi, K., Marin III, R., Mikulski, C., Pennington, J., Scholin, C., Smith, G., Woods, A., Zhang, Y., 2017. Causality of an extreme harmful algal bloom in Monterey Bay, California during the 2014–2016 northeast Pacific warm anomaly. Geophys. Res. Lett. <https://doi.org/10.1002/2017GL072637>.
- Rybczewski, R.R., Dunne, J.P., Sydemann, W.J., García-Reyes, M., Black, B.A., Bograd, S.J., 2015. Poleward displacement of coastal upwelling-favorable winds in the ocean's eastern boundary currents through the 21st century. Geophys. Res. Lett. 42, 6424–6431. <https://doi.org/10.1002/2015GL064694>.
- Saldías, G.S., Sobarzo, M., Quiñones, R., 2018. Freshwater structure and its seasonal variability off western Patagonia. Prog. Oceanogr. 0–1. <https://doi.org/10.1016/j.pocean.2018.10.014>.
- Schneider, W., Donoso, D., Garcés-Vargas, J., Escribano, R., 2017. Water-column cooling and sea surface salinity increase in the upwelling region off central-south Chile driven by a poleward displacement of the South Pacific High. Prog. Oceanogr. 151, 38–48. <https://doi.org/10.1016/j.pocean.2016.11.004>.
- Shaffer, G., Salinas, S., Pizarro, O., Vega, A., Hormazabal, S., 1995. Currents in the deep ocean off Chile (30°S). Deep Research. Part I 42, 425–436. [https://doi.org/10.1016/0967-0637\(95\)99823-6](https://doi.org/10.1016/0967-0637(95)99823-6).
- Sievers, H., Silva, N., 2008. Water Masses and Circulation in Austral Chilean Channels and Fjords. Progress in the Oceanographic Knowledge of Chilean Interior Waters, from Puerto Montt to Cape Horn. Comité Oceanográfico Nacional (CONA), Pontificia Universidad Católica de Valparaíso, pp. 53–58.
- Silva, N., Calvete, C., Sievers, H., 1997. Características oceanográficas físicas y químicas de canales australes chilenos entre Puerto Montt y laguna san rafael (cruceiro cimarfiorido 1). Ciencia Tecnología Marina 20, 23–106.
- Silva, N., Calvete, C., Sievers, H., 1998. Masas de agua y circulación general para algunos canales australes entre Puerto Montt y laguna San Rafael (Cruceiro CIMAR 1 Fjordos). Ciencia y Tecnología del Mar 21, 17–48.
- Silva, N., Neshyba, S., 1979. Note on the southernmost extension of the Peru-Chile undercurrent. Deep-Sea Res. I Oceanogr. Res. Pap. 26, 1387–1393.
- Silva, N., Palma, S., 2006. Avances en el conocimiento oceanográfico de las aguas interiores chilenas, Puerto Montt a Cabo de Hornos. Comité Oceanográfico Nacional, Valparaíso, Chile, pp. 162.
- Silva, N., Vargas, C.A., 2014. Hypoxia in Chilean Patagonian Fjords. Prog. Oceanogr. 129, 62–74. <https://doi.org/10.1016/j.pocean.2014.05.016>.
- Smith, M.D., Roheim, C.A., Crowder, L.B., Halpern, B.S., Turnipseed, M., Anderson, J.L., Asche, F., Bourillon, L., Guttormsen, A.G., Khan, A., Liguori, L.A., McNeven, A., O'Connor, M.I., Squires, D., Tyedmers, P., Brownstein, C., Carden, K., Klinger, D.H., Sagarin, R., Selkoe, K.A., 2010. Sustainability and global seafood. Science 327 (5967), 784–786. <https://doi.org/10.1126/science.1185345>.
- Spence, P., Griffies, S.M., England, M.H., Hogg, A.M., Saenko, O.A., Jourdain, N.C., 2014. Rapid subsurface warming and circulation changes of Antarctic coastal waters by poleward shifting winds. Geophys. Res. Lett. 41, 4601–4610. <https://doi.org/10.1002/2014GL060613>.
- Stramma, L., Peterson, R., Tomczak, M., 1995. The south Pacific current. J. Phys. Oceanogr. 1, 77–91. [https://doi.org/10.1175/1520-0485\(1995\)025<0077:tpsc>2.0.co;2](https://doi.org/10.1175/1520-0485(1995)025<0077:tpsc>2.0.co;2).
- Strub, P.T., Mesías, J.M., Montecino, V., Rutllant, J.A., Salinas, S., Robinson, A., Brink, K.H., 1998. Coastal ocean circulation off western South America. In: Robinson, A.R., Brink, K.H. (Eds.), The Sea. 11. John Wiley & Sons, New York, pp. 273–313.
- Sydemann, W.J., García-Reyes, M., Schoeman, D.S., Rybczewski, R.R., Thompson, S.A., Black, B.A., Bograd, S.J., 2014, jul. Climate change and wind intensification in coastal upwelling ecosystems. Science 345 (6192), 77–80. <https://doi.org/10.1126/science.1251635>.
- Thompson, D.W.J., Woodworth, J.D., 2014. Barotropic and Baroclinic annular variability in the southern hemisphere. J. Atmos. Sci. 71, 1480–1493. <https://doi.org/10.1175/JAS-D-13-0185.1>.

- Torrence, C., Compo, G., 1998. A practical guide to wavelet analysis. *Bull. Am. Meteorol. Soc.* 79, 61–78. [https://doi.org/10.1175/1520-0477\(1998\)079<0061:APGTWA>2.0.CO;2](https://doi.org/10.1175/1520-0477(1998)079<0061:APGTWA>2.0.CO;2).
- Torres, R., Pantoja, S., Harada, N., González, H.E., Daneri, G., Frangopulos, M., Rutllant, J.A., Duarte, C.M., Rúa-Halpern, S., Mayol, E., Fukasawa, M., 2011. Air-sea CO₂ fluxes along the coast of Chile: from CO₂ outgassing in central northern upwelling waters to CO₂ uptake in southern Patagonian fjords. *J. Geophys. Res.* 116, C09006. <https://doi.org/10.1029/2010JC006344>.
- Uppström, L.R., 1974. The boron/chlorinity ratio of deep-sea water from the Pacific Ocean. *Deep-Sea Res. Oceanogr. Abstr.* 21, 161–162. [https://doi.org/10.1016/0011-7471\(74\)90074-6](https://doi.org/10.1016/0011-7471(74)90074-6).
- Valle-Levinson, A., Sarkar, N., Sanay, R., Soto, D., Leon, J., 2007. Spatial structure of hydrography and flow in a Chilean fjord, Estuario Reloncaví. *Estuar. Coasts* 30, 113–126.
- Valle-Levinson, A., Wong, K.-C., 2000. Fortnightly variability in the transverse dynamics of a coastal plain estuary. *J. Geophys. Res.* 105, 3413–3424.
- Vargas, C.A., Lagos, N.A., Lardies, M.A., Duarte, C., Manríquez, P.H., Aguilera, V.M., Broitman, B.R., Widdicombe, S., Dupont, S., 2017. Species-specific responses to ocean acidification should account for local adaptation and adaptive plasticity. *Nat. Ecol. Evol.* 1, 0084. <https://doi.org/10.1038/s41559-017-0084>.
- Vargas, C.A., Martínez, R.A., San Martín, V., Aguayo, M., Silva, N., Torres, R., 2011. Allochthonous subsidies of organic matter across a lake-river-fjord landscape in the Chilean Patagonia: implications for marine zooplankton in inner fjord areas. *Cont. Shelf Res.* 31 (3-4), 187–201. <https://doi.org/10.1016/j.csr.2010.06.016>.
- Wang, B., Ding, Y., 1992. An overview of the Madden-Julian oscillation and its relation to monsoon and mid-latitude circulation. *Adv. Atmos. Sci.* 9, 93–111.
- Wentz, F.J., Scott, J., Hoffman, R., Leidner, M., Atlas, R., Ardizzone, J., 2015. Remote sensing systems cross-calibrated multi-platform (CCMP) 6-hourly ocean vector wind analysis product on 0.25 deg grid, version 2.0. Remote Sens. Syst. www.remss.com/measurements/ccmp/.